U. S. DEPARTMENT OF THE INTERIOR
U. S. GEOLOGICAL SURVEY

Basin evolution, and the timing and extent of oil generation, Canning River region, North Slope, Alaska: Preliminary Basin2 calculations assuming a conductive thermal history

By

Elisabeth L. Rowan

Open-file Report 97-711

CONTENTS

Basin evolution, and the timing and extent of oil generation, Canning River region, North Slope, Alaska: Preliminary Basin2 calculations assuming a conductive thermal history

Elisabeth L. Rowan

INTRODUCTION

This investigation was undertaken as part of a petroleum resource assessment of the coastal plain or "1002" region of the Arctic National Wildlife Refuge (ANWR) on Alaska's North Slope (Bird et al., in prep.). ANWR is on federal land in a region potentially rich in oil and gas. The Prudhoe Bay oil fields lie to the west of ANWR and the MacKenzie Delta fields to the east in Canada, both with many geologically and tectonically similar environments. Recent advances in computer capabilities have made possible numerical simulations that integrate knowledge of the region's geologic history, and permit 'prediction' of the resulting thermal and hydrologic history. In this report, only vertical fluid flow is considered and heat conduction is assumed to be the dominant control on the thermal regime. This report's primary goal is to evaluate the timing and extent of thermal maturation of petroleum source rocks in the 1002 region, based on simulations of burial and thermal history. The timing of oil generation, combined with a history of the basin's geometry, the regional dip of carrier beds, and formation of traps and seals permit geologists to assess the likelihood that oil accumulations currently exist in a given region. Two principal source rocks are represented in the 1002 region, the Shublik Formation (Triassic) and the Hue Shale (Cretaceous). The Mikkelsen Tongue of the Canning Formation (Eocene) is postulated as a source rock in more distal (offshore) settings. The thermal history calculated for these source rocks is a byproduct of a more comprehensive simulation of the North Slope basin's evolution at the Canning River. Measurements of vitrinite reflectance and apatite fission track ages help to constrain the geologic history when the stratigraphic record is missing.

The North Slope of Alaska consists of a foreland basin whose southern margin, the Brooks Range, is an active fold and thrust belt. This report presents results for a 90 km north-

south cross-section along the Canning River, in a relatively undeformed part of the coastal plain. In this area the Canning River forms the western margin of ANWR; the cross-section is based on observations and data collected from eight wells in the vicinity of the river (Fig. 1). Additional work on N-S and E-W sections offshore are in progress.

An undeformed section was selected because the software for modeling the basin's evolution, Basin2, does not simulate faulting. The Canning River section has been uplifted and eroded, but unlike much of the 1002 region has experienced relatively little thrust faulting. Another factor favoring the section was the availability of published geologic cross-sections and data from wells drilled along the Canning River. Well data is lacking from the 1002 area proper although numerous seismic reflection profiles and some outcrop information are available.

Several studies have been published of fluid flow, heat flow and thermal maturity on Alaska's North Slope. Deming et al. (1992) and Deming (1993) described present day surface heat flow patterns on the coastal plain of the National Petroleum Reserve in Alaska (NPRA) west of Prudhoe Bay, in the context of topographically driven regional flow. This work is essential to an understanding of North Slope hydrogeology, and its possible effects on petroleum distribution, but does not address the timing of oil generation. Magoon and others (1987) have evaluated the thermal maturity of source rocks in ANWR using the Lopatin method.

The current report examines oil source rock maturities in the 1002 region along the Canning River section using first order rate law kinetics (Tissot and Welte, 1984) to describe the kerogen-liquid petroleum transformation. Simulating the burial history of an entire cross-section provides a useful summary of the section's tectonic and geologic history. The program demands consistent input for every specified well and time interval, making gaps in knowledge immediately apparent. The basin evolution described here will serve as essential groundwork for a more complete investigation of the region's hydrology and hydrocarbon history; details of the model input and the methodology are included for use as a reference in future work.

GEOLOGIC/GEOPHYSICAL INPUT TO THE MODEL: SUMMARY AND REFERENCE INFORMATION

Introduction

The Canning River section's burial and thermal history were simulated with Basin2, a program designed for numerical solution of coupled sediment deformation, fluid flow, and heat flow equations. A complete description of the program is presented in Bethke et al. (1993). This preliminary investigation addresses only the conductive thermal history of the Canning River section. Formation thicknesses and lithologic compositions comprise basic input for the model. One of the challenges was estimating the thickness of formations now completely removed by erosion, as with the Kingak Shale north of Beli well. The stratigraphic record defined in the Canning River (1002) model begins with the pre-Mississippian basement rock and continues to the present day. Strata below the Triassic Shublik Formation, the oldest oil source rock, are unlikely to have had a significant effect on the conductive thermal history of the overlying rocks, but are included to provide a more complete summary of the region's geologic history.

Well locations and stratigraphic control

Eight wells along the Canning River and offshore provide the stratigraphic control for the Basin2 cross-section (Fig. 1). From south to north the wells are Canning River A-1, Canning River B-1, Beli, Alaska State J-1, Leffingwell, West Staines State-2, Point Thomson-1, and Hammerhead-1. A geologic cross-section (Bird and Magoon, 1987, Plate 1) provided the basic geologic input, updated with revised, unpublished cross-sections compiled by Bird (written comm.). The stratigraphic section is described in Basin2 as a series of time-stratigraphic intervals, including unconformities (Table 1). Formation thicknesses were measured from the cross-sections and entered in the Basin2 input file. The program "backstrips" each formation based on the compaction properties of the rock-type.

In regions of extensive erosion, particularly in the south where uplift is greatest, sediment thicknesses were estimated maintaining a 'reasonable' geometry over the entire section. In most cases, trends of increasing or decreasing thickness were extrapolated to maintain a constant rate of change with distance. Vitrinite reflectance and apatite fission track measurements provided important additional constraints. Amounts and rates of burial and uplift were adjusted so as to match these data as closely as possible.

Apatite fission track analyses

Apatite fission track (AFT) analyses by O'Sullivan et al. (1993) constrain the magnitude and timing of uplift and erosion. In general, deformation and uplift are greatest in the fold and thrust belt to the south (the Sadlerochit Mountains in ANWR) and decreases northward. Sedimentation prior to uplift was defined in part in the Basin2 model as an amount sufficient to raise temperature at the fission track sample sites to at least 90°C, the approximate closure temperature. With subsequent erosion, the samples cooled through their closure temperatures.

Other physical parameters

Other physical parameters that affect the thermal history calculations include heat flow, surface temperature, and water depth (i.e. depth from sea level to sediment-water interface).

Heat flow. In Basin2 heat flow from the basement can be varied both in space and time. Heat flow was adjusted as the final step in attempting to match calculated vitrinite reflectances with measured values. Heat flow was allowed to vary from 1.25 to 1.5 HFU (52 to 62.5 mW/m^2) along the cross-section (see Table 2); the continental average is 1.5 HFU.

No heat flow measurements or calculations are available in the 1002 area, although Deming et al. (1993) calculated heat flows from temperature measurements in the NPRA. On

the NPRA coastal plain, calculated values range from about 50 to 90 mW/m^2 Deming et al., 1993, fig. 6). The highest heat flow are presumably the result of focused fluid flow over the Barrow Arch. Deming et al. (1993, fig. 6) report values as low as 40 mW/m^2 in the mountains to the south. The pattern of depressed temperatures in the elevated recharge zone and high temperatures at the discharge zone is characteristic of topographically driven flow systems. It is possible that the Canning River section had sufficient north-south extent to have intersected zones of significant recharge and discharge and experienced similar thermal effects.

Surface temperature. Average surface temperature varied considerably over time from a high of about 20°C in the Pennsylvanian to below zero present day (Table 2) (McSweeney, 1993). Temperatures below 0°C have prevailed on the North Slope since the Pleistocene and present a problem because Basin2 does not accept values below about 0.5°C. In the Canning River model surface temperatures of 0.5°C are specified beginning in mid-Miocene (Table 2). These values exceed present day measured surface temperatures on the North Slope which range from -4.6° to -12.5°C (Lachenbruch et al., 1988; Collett et al., 1993, Table 1).

Including permafrost in the model would permit a partial 'work around' to the temperature limitation in Basin2. Ultimately permafrost was entirely omitted due to difficulties with numerical stability and with the plotting routine, but will be included in future work.

Ice-bearing permafrost is defined here as the surficial zone in which pore water is frozen; other definitions specify only that temperatures must be ≤0°C. Ice-bearing permafrost reaches thicknesses as great as 2000 feet over much of the North Slope coastal plain. Depths to the base of the ice-bearing permafrost are reported in Collett (written notes, April, 1996). To represent a permafrost layer without changing the thickness of the sedimentary section, the model should specify rapid erosion of 2000 ft. of sediment at Leffingwell, thinning to zero at Hammerhead well and at Beli well (model unit 18, Table 2). The eroded sediments would then be replaced with a layer (model unit 19) with different physical properties, low permeability and high thermal conductivity so that temperature across the layer is uniform. In the model the

surface temperature of 0.5°C would then be essentially fixed at the base of the permafrost. Measured temperatures at the base of the permafrost range from -0.3° to -3.8°C (Collett et al., 1993, Table 2). After including the 'work around' the discrepancy between measured and model temperatures would generally be less than 5°C at the base of the permafrost, greatly reduced from the 4-12°C discrepancy at the surface. The relatively short duration of temperature discrepancies minimizes their impact on maturities of organic matter, however including permafrost will permit calculation of present day depth-temperature profiles. Comparison with measured surface and bottom hole temperatures from wells would provide an additional check on the accuracy of the model's predictions. In the current model, vitrinite reflectance and apatite fission track measurements provide the only verification of thermal history.

Water depth. Water depth has minor effects on the rocks' temperature profile with depth. Negative values for water depth in Basin2 indicate elevations above sea level and are useful in defining topography. When water depth is constant, accumulation of sediment must be accompanied by equivalent basement subsidence. Paleo-water depth is relatively well known for the Cretaceous based on amplitudes of seismic clinoforms; warm temperatures during this interglacial period resulted in high sea levels world-wide and an estimated water depth of about 1 km in the study area. Sea levels during deposition of the Jurassic Kingak Shale are estimated to have been approximately 150 m (F. Cole, written comm.). In the remaining time intervals paleo-water depths are less well known. When marine conditions prevailed a water depth of 30 m was specified to represent the depositional environment of shallow marine shelf rocks. Water depths of zero are specified for terrestrial rocks (Table 2).

Rock Properties

Lithologies and 'end member' rock types. Each stratigraphic unit in the Canning River cross-section was assigned a lithology represented as a compositional mixture of three

end members, sandstone, shale, and carbonate. The units in the model were lithologically uniform even though spatial variation in composition is permitted in Basin2. Table 3 summarizes physical properties of the three end member rock types. When a formation is composed of more than one of the end member rock types, physical properties are averaged. In this report, and by default in Basin2, an arithmetic average is used in the x-direction, along stratigraphy, but a harmonic average is used in the vertical direction. Only relatively small changes have been made to the default values built into Basin2. Future work should investigate whether tailoring the rock properties to more closely match those of ANWR lithologies would significantly change the model results.

Compilations of data from well logs are the primary source of lithologic information for the Tertiary units and for the Lisburne Group. Lithologies for the remainder of the section are based on stratigraphic columns published in Magoon et al. (1987, Appendix 11.1). The table below was excerpted from notes by Phil Nelson (written comm., 4/97) and contains information used to define the model lithologies listed in Table 2.

Thickness (feet) of selected reservoir-prone formations, from well log criteria. No cutoff criterion for porosity has yet been applied.

Formation/Group	# wells	Avg. Gross	Avg. Net	Initial Net/Gross
Saganavirtok	11	2626	778	0.30
Staines Tongue of Sag.	6	1223	491	0.50
Mikk. Tongue of Cann.	7	3095	380	0.14
Canning	10	2658	301	0.13
Lisburne	3	1860	1612	0.86

'Avg. Gross' is the formation thickness, and 'Avg. Net' is the average thickness of rocks with reservoir potential, i.e. sandstone, or carbonate in the Lisburne Group. Initial Net/Gross ratio is the sandstone (or carbonate) fraction of the formation.

The following assumptions were made in order to calculate overall sandstone:shale:carbonate ratios for each stratigraphic unit. 1) The composition of the non-reservoir fraction in each interval was assumed to be siltstone and shale with a ratio equal to the Initial Net/Gross ratio. 2) Siltstone was assumed to be composed of fine sand and shale in equal proportions.

In the case of the Staines Tongue of the Sagavanirtok Formation (Paleocene) and the Paleocene part of the Canning Formation an average Initial Net/Gross ratio was calculated, weighted by the thickness of the formation. A weighted average Initial Net/Gross of 0.25 was used to represent the Paleocene unit in the model (unit 11) for the 7 southernmost wells. In Hammerhead well the Canning lithologic ratios were used because the Staines Tongue pinches out between Pt. Thomson and Hammerhead.

Porosity. Basin2 "backstrips" or adjusts the thickness of each formation thickness to account for porosity loss during burial and porosity rebound resulting from erosion and uplift. Porosity (ϕ) is assumed to be high when sediments are initially deposited, but is rapidly reduced during progressive sedimentation and loading. The relationship between porosity and depth (Z) is defined as:

$$\phi = \phi_0 e^{-bZ} + \phi_1$$

where ϕ_0 is the reducible porosity present when the sediment is deposited, ϕ_1 is irreducible, minimum porosity, and b is a compaction coefficient defined for each rock type (Table 3.). The larger the value of b the more rapidly the sediments compact with burial (Bethke et al., 1993).

The relationship between porosity and depth is most easily expressed as:

$$\ln(\phi-\phi_1) = -bZ + \phi_0$$

The compaction coefficient can be empirically determined by assuming a value for ϕ_1, plotting $\ln(\phi-\phi_1)$ vs. Z from paired measurements of ϕ and Z. The best fit slope through the data gives a line whose negative slope is b and intercept is ϕ_0 (Bethke et al., 1993). In future work, compaction coefficients may be verified or refined using this equation and measurements of porosity and depth.

In Basin2 an unloading coefficient, bul, controls the amount of porosity rebound during uplift and erosion. Values for bul listed in Table 3 are 20% of the compaction coefficient, indicating that 20% of porosity lost would be regained during complete unloading.

Density. The density of the porous medium is calculated as the weighted average of the densities of water and of the minerals in each rock type. Densities for sandstone, shale, and carbonate are listed in Table 3. As with other variables, mineral densities may be defined to fit observations and data. Water densities are discussed below.

Permeability. Permeability (k) is usually correlated with porosity (ϕ) in sedimentary rocks. In the horizontal direction the relationship is empirically defined as: $\log k_x = A\phi + B$. Coefficients A and B are the slope and intercept of a least squares fit to a plot of log permeability vs. porosity and define distinct relationships for each rock type (Table 3). Vertical permeability, kz, is calculated from pre-defined anisotropy values, kx/kz (Table 3). To facilitate calculations, only the vertical component of flow resulting from compation was considered. Permeability potentially affects temperatures through its affect on fluid flwo rates and advective heat transport. However, given only vertical flow and slow flow rates, permeability did not significantly influence the conductive regime assumed in the current model. In future work addressing regional topographically driven flow, permeabilities will play an important role in determining flow rates.

Thermal properties of the porous medium

Thermal conductivity. Thermal conductivity (K), like permeability, is calculated as a function of porosity. Large differences (factor of 4) in the conductivities of minerals versus water (Table 3) make porosity a key factor in determining the medium's bulk conductivity. The relationship is defined as: $K = A_{tc}\phi + B_{tc}$. A_{tc} and B_{tc} are the slope and intercept of a least squares fit to a plot of conductivity vs. porosity (Table 3).

Heat capacity. The heat capacity of the porous medium is calculated from the weighted volumetric average of values for the rock grains and water. The heat capacity of the mineral grains is a function of temperature defined in Basin2 by an extended form of the Maier-Kelley equation (see Bethke et al., 1993). This equation is unnecessarily precise however, it is compatible with thermodynamic databases that list the coefficients for a large number of minerals.

Fluid Properties

Basin2 determines physical properties of water as a function of temperature, pressure and salinity using the data and correlations of Phillips et al. (1980; 1981). The fluid density correlation is accurate in the temperature range 0-350°C, 0.25-5 molal NaCl, and from pressures <50 MPa (Mega-Pascals) to greater than the fluid's vapor pressure. Basin2 extrapolates density calculations to salinities of 12 molal. The fluid's coefficients of isothermal compressibility and isobaric thermal expansion are derived from the change in density with temperature and pressure. Heat capacities are determined from enthalpies tabulated for an 0.5 molal NaCl solution from 0°-300°C. Basin2 maintains look-up tables for NaCl solubility as a function of temperature and for viscosity as a function of both temperature and salinity.

The variability of fluid properties with temperature has little affect on the present calculations where a conductive thermal regime is assumed, but would become very significant when ground water flow is addressed. In the current model salinity is assumed constant at sea water concentration, approximately 0.5 molal. Future investigation of topographically driven flow may incorporate variable salinity where fresh water is recharged in the mountains and mixes with deep basin brines.

Maturation of Organic Matter

The three potential hydrocarbon source rocks in ANWR are the Upper Triassic Shublik Formation, the Upper Cretaceous Hue Shale, and the Eocene Mikkelsen Tongue of the Canning Formation. The extent of transformation of kerogen to petroleum in the source rocks

is of primary interest in this report, but vitrinite reflectances provide important constraints on the thermal history. Basin2 uses a standard approach and equations (Tissot and Welte, 1984; Lewan, 1985) to calculate a petroleum transformation ratio, and uses the parallel reaction model of Sweeney and Burnham (1990) to calculate vitrinite reflectance.

The rate at which kerogen is transformed to liquid petroleum is defined by a first order rate law:

$$dX_O/dt = k(1-X_O)$$

where t is time, and X_O is oil generated as a fraction of the rock's total oil generating capacity. The rate constant (k) is given by an Arrhenius equation:

$$k = A_O e^{-E_a/RT_K}$$

where A_O and E_a are the pre-exponential factor and activation energy, respectively; T_K is temperature in Kelvins, and R is the gas constant.

Basin2 calculates the extent of oil generation using a single pair of kinetic constants, A_O and E_a, specified for a given source rock. When the kerogen in a source rock can be adequately characterized by a pair of A_O and E_a values, as in the case of the Shublik Formation and Hue Shale, the extent of oil generation can be readily calculated as a fraction of total generating potential, i.e. normalized to one. Kinetic constants for the Shublik Formation and Hue Shale were determined based on analyses of organic sulfur/carbon ratios and assuming pure Type II kerogen (Lillis, written comm., 5/16/97).

Kerogen in the Mikkelsen Tongue, primarily Type III, is more heterogeneous. Values for the Eocene Richards Formation, the Mikkelsen's lateral equivalent in the MacKenzie Delta, serve as a 'best estimate' although they represent activation energies for only 60% of the formation's kerogen (Issler and Snowdon, 1990). The oil generation calculation was carried out using constants for the Richards Formation, and was repeated using constants for the Phosphoria Retort Shale. These represent the best available values and the 'fast' end of possible range of values for the Mikkelsen Tongue. Table 4 lists kinetic constants for the source rocks of ANWR and values for comparison from several other localities. Hydrous

pyrolysis analyses planned for the future should provide more accurate kinetic constants for the Mikkelsen Tongue in ANWR.

Numerical Modeling: Configuring and running Basin2

Basin2 program. Basin2 is a 2-D numerical program that solves coupled equations for fluid and heat flow, and for evolution of porosity and fluid pressure as a function of burial history in a sedimentary basin. The original version written by Craig Bethke in 1982 has been extensively revised with assistance from students and staff at the University of Illinois (Bethke et al., 1993).

Pressure and temperature distributions can be carried out at several levels of complexity. The current ANWR model assumes that heat transfer occurred by conduction only and that fluid movement occurred only in a vertical direction. Vertical flow allows calculations of pressures and flows resulting from sedimentation and porosity collapse, however advective heat transfer by ground water movement is not considered. The calculation for flow in two dimensions, fully coupled with heat transport, was numerically unstable and could not be pursued with the current model configuration.

Grid. Basin2 takes input in the form of vertical cross-sections, discretized as a finite difference grid. The width of the cross-section in this model is 90 km. Thirty columns are specified and have a uniform width of 3 km across the grid. The number of rows varies over time due to sedimentation and erosion and cell heights vary with the thickness of the stratigraphic unit. The physical properties of each cell is defined for the nodal point at the center of the cell. In the calculations that follow, references are made to individual nodes, identified by the column and row number. Column one is located at the southern end of the cross-section and column 30 at the northern end. Row numbers begin with one in the basement and increase upwards.

Boundary and initial conditions for Canning River section. Thermal and pressure boundary conditions may be constant over time or may be redefined for individual time/stratigraphic intervals. The program linearly interpolates boundary conditions for any time interval from conditions prevailing at the end of the previous interval. Thus for example, surface temperature decreases linearly over time from 19.5°C at the end of the Triassic to 12°C at the end of the Jurassic (see Table 2, model units 6 and 7).

Boundary conditions defined in this report can be summarized as follows.

Top. Pressure/head: 1 ATM., water table is assumed to be at the ground surface. Temperature: specified and varies with time interval (Table 2).

Bottom: Closed to fluid flow; specified heat flux varies with time interval (Table 2).

Sides: "Open". Pressure is fixed at hydrostatic values calculated from the pressure/head condition at the ground surface. Temperature is fixed at values defined by a vertical heat conduction.

Initial conditions in this study were hydrostatic pressure, and temperature calculated for a conductive thermal regime.

Transient vs. Steady state calculations. Steady state calculations give the temperature and pressure distributions that would result if the system were perfectly equilibrated; time is not considered. In transient calculations the system adjusts, from initial conditions towards equilibrium. Pressure and temperature are permitted to change by only in small increments (e.g., 1°C, and 1 atm.) in a given time step, and time steps are reduced until this condition is met. Transient calculations are needed to calculate thermal maturities which are a function of time as well as temperature.

Steady state solutions were used in preliminary calculations of overpressures and ground water flow resulting from topography. Transient calculations of these processes can be time-consuming, up to several days per simulation, but will be pursued in future work.

BURIAL AND THERMAL HISTORY MODEL: CALCULATIONS AND RESULTS

Summary of Geologic History

A series of cross-sections illustrate key 'time slices' (Figs. 2a-i) and captions briefly summarize the region's geologic and tectonic history. Shale fraction was chosen as the color-mapped variable because the range of values allows several important units such as the Mikkelsen Tongue, the Hue Shale, and Kingak Shale to be easily identified.

Calculations vs. observations

Temperatures. Temperatures for the ANWR region are limited to surface and bottom hole measurements. Permafrost, discussed above, is omitted the model, but deserves further attention as a means of checking that the model accurately reproduces present day temperatures at specific locations in the cross-section. Apatite fission track (AFT) analyses provide constraints on paleotemperature at two sites (Fig. 3). No fluid inclusion measurements are available.

AFT measurements indicate the times at which samples passed through the apatite's closure temperature. Paleocene and early Eocene sedimentation was assumed to have been great enough prior to uplift to produce temperatures sufficient to reset the fission tracks. Figure 4 shows the burial history of nodes with the same approximate location as the AFT samples, and Figure 5 shows the evolution of temperature over time at these sites. Approximately 4.5 km of erosion apparently resulted from uplift at the southern end of the cross-section during Eocene and Oligocene time. Uplift and cooling rates are highest for the southernmost sample (Node 1,9, near A-1 well) because this site was more deeply buried and underwent greater uplift (Fig. 4).

If AFT closure temperatures are assumed to decrease as cooling rates slow, then the deeper sample near well A-1 would have been reset at a slightly higher temperature (~95°C) and the shallower sample located near well B-1 would have a lower resetting temperature

(~85°C) (see Faure, 1986, ch. 20). Under these assumptions, both samples would have been reset at about the same time, approximately 44.5 m.y. b.p. On the other hand, if one assumes a fixed closure temperature, as did O'Sullivan et al. (1993), the deeper sample (Node 1,9) is reset distinctly earlier than the shallower sample (Fig. 5). For a closure temperature of about 100°C the samples would be reset at 46.5 and 44.5 m.y., in fairly good agreement with the 46 and 43 m.y. resetting ages indicated by O'Sullivan et al. (1993, their Fig. 4).

In these calculations erosion is assumed to occur at the same rate as uplift and the sediment surface is assumed to be at sea level. Clearly there must have been topography throughout the region's history, but there is virtually no information with which to estimate values. Given that uplift is occurring currently, present day elevations should give some idea of the range of elevations likely to have prevailed during past episodes of uplift. Beli well, the current highest point along the Canning River section is at 1022 ft.; elevations in the Sadlerochit Mountains are on the order of 4000 ft. Although the assumption of zero topography was considered preferable to an unconstrained guess, it implies a cooling rate that is greater than the actual value.

Vitrinite reflectance. Vitrinite reflectance measurements made on drill core and outcrop samples (Johnsson et al., 1992; Bird et al., in prep.) represent the only means of verifying that the model accurately reproduces the thermal history of the Canning River section. A good match provides evidence that the model does reproduce the region's thermal history, independent of whether the processes leading to this history are correctly simulated. Considerable effort was made to bring the calculated vitrinite reflectances into reasonable agreement with measured values (Figs. 6 a-c).

The poorest match is between calculated and measured values at well A-1 (Fig. 6a). The slope of the calculated profile is too shallow to match most of the data, yet it is roughly parallel with the measured and calculated profiles in the adjacent well, B-1. The data at A-1 show remarkably little increase in maturity over most of the depth range, raising some question

as to their validity. Slightly reduced heat flow would have improved the match at A-1, but would have worsened the match at B-1. Under the current assumption of normal heat flow at all but J-1 and Leffingwell, the calculated curve at B-1 is slightly below a 'best fit' curve but still within well within the range of the measurements. Given the many sources of uncertainty the match is remarkably good at the remaining wells (Figs. 6a and b).

Initial vitrinite reflectance calculations were made using the Basin2 default values for porosity, thermal conductivity and basement heat flow. Under these assumptions values were generally too low near the surface and too high at depth to match the data. The first step in improving the match was to reduce the thermal gradient by increasing thermal conductivity throughout the section. This was accomplished by 1) increasing the shale and sandstone conductivities by about 15% (Table 3), and 2) by reducing both initial and irreducible porosities to the values listed in Table 3. Conductivities and porosities are still within the normal ranges for these rock types. In a study of MacKenzie River delta shales Issler (1992) reported initial porosities that bracket the initial shale porosities assumed here.

Lower porosity increases *bulk* thermal conductivity because water, with its low conductivity, occupies a smaller fraction of the rock. With these changes, the vitrinite-depth profiles had roughly the correct slope but still did not match well with observations at J-1 and Leffingwell. Heat flow was reduced from 1.5 HFU (62.5 mW/m^2), the continental average, to 1.25 HFU at J-1 and Leffingwell (Table 2).

In tectonically active regions rapid uplift or subsidence of the order of mm/year may alter the equilibrium geothermal gradient and heat flow. Heat flow in a subsiding basin where cool sediment is accumulating rapidly will have a below average thermal gradient and depressed heat flow until thermal equilibrium can be established. Low heat flows are shown to correspond to rapid sedimentation rates in the Gulf of Lions basin (Burrus and Audebert, 1990), and offshore to the north of Holland where values as low as 41 mW/m^2 (1 HFU) are reported for the more rapidly subsiding basins (Verweij, 1997).

In the Canning River section, the region where lowest heat flow was required, Leffingwell and J-1 wells, is also the region of greatest Tertiary sedimentation unaffected by subsequent uplift. Sedimentation rates of 0.2-0.3 mm/yr may have had a transient affect on thermal gradients and may explain the anomalously low vitrinite reflectances. It has been suggested that the short distance over which heat flow appears to vary (tens of km) is better explained by hydrologic processes than by heterogeneities in heat flow from the upper mantle. This seems intuitively correct, but does not address the transient thermal effects of rapid sedimentation.

The relatively modest decrease in specified heat flow from the continental average appears to reproduce the effect of rapid subsidence but without simulating the underlying cause. Due to practical limitations, heat flow in the current model is fixed at the base of the sedimentary section, at depths of 5 km or less. Thus transient heat flow variations due to deformation and heterogeneities in the upper crust cannot be simulated. If the bottom grid boundary were placed several kilometers deeper, the thermal effects of rapid subsidence, for example, could probably be reproduced in the simulations.

Topographically driven fluid flow can be shown to produce a thermal pattern in which temperatures are depressed in the uplifted recharge area and elevated in the discharge zone (e.g., Deming et al., 1992). The crest of the Sadlerochit Mountain range lies tens of kilometers to the south of Leffingwell and J-1 (Fig. 1) and these wells may have had depressed temperatures as a result of regional flow. Whether or not this is the case, the cool temperatures associated with recharge are unlikely to have altered vitrinite reflectance values.

Timing of Source Rock Maturation

Oil generation as a fraction of total generating capacity has been calculated for three source rocks, the Upper Triassic Shublik Formation, the Upper Cretaceous Hue Shale, and the Eocene Mikkelsen Tongue of the Canning Formation The burial history determined from stratigraphy and assumptions made for the thermal properties of the rocks define a thermal

history that reproduces observed vitrinite reflectance values relatively well. This thermal history also determines the rate and degree of oil generation calculated for the oil source rocks.

To the south, the onset of oil generation would have occurred earlier than in the Canning River section due to deeper burial. However, extrapolating the timing of generation southward from well A-1 is complicated by the increased structural complexity. The time-temperature history of the region south of the Canning River section is probably best undertaken by a structural reconstruction combined with calculations of the resulting conductive thermal regime, using a program designed for structurally deformed regions (e.g., Thrustpak).

Shublik Formation The calculations indicate that oil was generated from the Shublik Formation throughout its extent in the Canning River section. Based on the best available kinetic constants (Table 4) significant oil generation began in the earliest Tertiary at about 65 m.y. at the southern end of the section and shifted northwards over time (Fig. 7a). Generation had virtually ceased by the end of Eocene uplift and erosion at about 37 m.y. (Fig. 2f). The Shublik has generated 100% of it's capacity at A-1 well, but significant (>30%) generation potential remains north of B-1 well.

The calculations were duplicated using the kinetic constants determined for the Phosphoria Shale which represent the extreme 'fast' end of the range of possible values (Table 4). Results based on the Phosphoria constants give the maximum fraction of oil generation that could be expected (Figure 7b).

Hue Shale. Oil generation in the Hue Shale has also been calculated using two sets of kinetic constants (Table 4). Using the best available constants, significant generation begins in the Early Tertiary at about 55 m.y. and shifts northwards with time (Fig. 8a). As with the Shublik generation has ceased by about 37 m.y. However even at the southern end of the cross-section, the Hue has generated only a small fraction (~1%) of its total capacity (Fig. 8a).

Using the 'fast' Phosphoria constants the calculations indicate a much higher total fraction of oil generation (Fig. 8b). Vitrinite reflectance values calculated for different geographic locations within the Hue Shale provide an interesting comparison and indicate that most of the formation falls within the oil window, defined as $0.6 \geq Ro \leq 1.2$ (Fig. 9).

Mikkelsen Tongue. Negligible amounts of oil generation were predicted for the Mikkelsen Tongue using the best available kinetic constants (Table 4). Using the 'fast' Phosphoria constants a small amount of oil generation, approximately 10% of total capacity, was predicted at the northern end of the cross-section where the Mikkelsen Tongue has been most deeply buried (Fig. 10). Even this fraction however could be volumetrically significant if the volume of rock involved were large and the source rock organically rich.

DISCUSSION

The burial and conductive thermal history detailed in this report provides groundwork for investigation of the region's hydrogeologic history. Preliminary steady state calculations indicate that substantial overpressures developed in the Tertiary, particularly during intervals of rapid sedimentation in Eocene and Miocene time. Overpressures can affect regional flow patterns and reduce the thermal conductivity of the affected rock by increasing its porosity and water content. Although not explicitly treated by Basin2, hydraulic fracturing induced by overpressuring can play a role in both primary and secondary petroleum migration.

Topography in the Sadlerochit Mountains may have created an important hydrodynamic drive for northward ground water flow. Folding and faulting created significant topography and therefore a hydraulic head gradient away from the crest of the Sadlerochit range. Several factors that might have reduced the effects of topographically driven flow include 1) low rates of meteoric recharge, i.e. little snow or rainfall, in the mountains, 2) low vertical permeability and low infiltration rates across bedding and particularly across thrust planes in the mountain belt, and 3) the possible presence of permafrost in the Sadlerochit

Mountains. If continuous over a wide area, the permafrost's low permeability would greatly reduce the rate of meteoric recharge to the flow system. However permafrost has been present for about 2 m.y., a fraction of the approximately 20 m.y. that the area has been uplifted.

Steady state calculations show that given sufficient recharge the elevation of the Sadlerochit mountains would create vigorous northward flow. Fold and thrust mountain belts in more temperate climates are thought to serve as recharge zones for regional flow systems; examples include the Rocky Mountain thrust belt in Idaho-Wyoming (Burtner and Nigrini, 1994; Burtner et al., 1994), and in Alberta, Canada (Hitchon, 1984), and the Ouachita thrust belt in Arkansas (Bethke and Marshak, 1990). To the west of the 1002 region Deming et al. (1992) provide present-day heat flow evidence that meteoric recharge in the Brooks Range created a northward regional flow system through the North Slope basin. To the east in the Beaufort-MacKenzie Basin, Canada, Hitchon et al. (1990) provide geochemical evidence that formation waters were flushed and replaced by meteoric waters to a depth of at least 2 km. The flushing took place at the end of the Miocene coincident with uplift and erosion in the mountain belt to the south. It seems likely that flushing of the formation waters actually resulted from topographically driven flow.

Topographically driven ground water flow may have played a role in the migration of oil; in general it would tend to sweep oil northwards. The most pronounced thermal effects in a topographically driven flow system are a depressed thermal gradient in the recharge area and an elevated gradient at the discharge region. The Canning River section comprises a portion of the total flow path and may not necessarily have experienced these thermal effects to a significant degree. A detailed analysis would require knowledge of the timing and amount of uplift in the mountain ranges based on a structural reconstruction of the mountain belt. This would permit quantitative modeling of the rate, duration, and thermal effects of fluid flow.

Buoyant forces may either have opposed or acted in the same direction as ground water flow. Buoyancy is always directed updip, and its magnitude can be determined from the oil-water density contrast and the dip angle of the carrier bed. Hayba and Bethke (1995), for

example, use this approach to determine the direction and rate of oil migration in the Los Angeles basin. Thus buoyancy is likely to have driven oil migration northward onto the northern flank of the North Slope basin until Eocene uplift at about 37 m.y. (Figs. 2d-f). Following uplift buoyancy may also have driven oil southwards into the upturned, thrust-faulted beds of the Sadlerochit Mountains (Figs. 2f-i), depending on the location of oil generation. By the end of the Tertiary the regional dip is northward, except locally near the Barrow Arch (Fig. 2i). Clearly, a 3-dimensional basin reconstruction is needed to provide a complete analysis of dip directions and likely oil migration paths due to buoyancy. The combined role of buoyancy and hydrodynamic flow in redistributing oil in the ANWR region remains an important question.

Acknowledgments

Simulation of the North Slope basin's evolution was based on information from many sources. Valuable discussions and input from Ken Bird, Bob Burruss, Fran Cole, Tim Collett, John Grace, Dan Hayba, David Houseknecht, Paul Lillis, Les Magoon, Tom Moore, John Murphy, and Phil Nelson are gratefully acknowledged.

REFERENCES CITED

Berggren, W.A., Kent, D.V., Swisher, C.C., Aubry, M.P., 1995, A revised Cenozoic geochronology and chronostratigraphy, Geochronology Time Scales and Global Stratigraphic Correlation, SEPM (Society for Sedimentary Geology), p. 129-212.

Bethke, C.M., and Marshak, S., 1990, Brine migrations across north America -- The plate tectonics of groundwater: Annual Review of Earth and Planetary Science, v. 18, p. 287-315.

Bethke, C.B., Lee, M.K., Quinodoz, H.A.M., Kreiling, W.N., 1993, Basin modeling with Basin2: Urbana, Illinois, The University of Illinois, 225 p.

Bird, K.J., Bader, J.W., 1987, Regional geologic setting and history of petroleum exploration, in Bird, K.J., Magoon, L.B., ed., Petroleum Geology of the Northern Part of the Arctic National Wildlife Refuge, Northeastern Alaska, U.S. Geological Survery Bulletin 1778, Chapter 3, p. 17-25.

Bird, K.J., and others, Assessment of Petroleum Resources of ANWR (1002 Region), North Slope, Alaska, U. S. Geological Survey, in prep.

Burtner, R.L., Nigrini, A., 1994, Thermochronology of the Idaho-Wyoming Thrust Belt during the Sevier Orogeny: A new, calibrated multi-process thermal model: American Association of Petroleum Geologists Bulletin, v. 78, p. 1586-1612.

Burtner, R.L., Nigrini, A., Donelick, R.A., 1994, Thermochronology of Lower Cretaceous Source Rocks in the Idaho-Wyoming Thrust Belt: American Association of Petroleum Geologists Bulletin, v. 78, p. 1613-1636.

Burrus, J., and Audebert, F., 1990, Thermal and compaction processes in a young rifted basin containing evaporites: Gulf of Lions, France: American Association of Petroleum Geologists, v. 74, p. 1420-1440.

Collett, T.S., Bird, K.J., Magoon, L.B., 1993, Subsurface temperatures and geothermal gradients on the North Slope of Alaska: Cold Regions Science and Technology, v. 21, p. 275-293.

Deming, D., Sass, J.H., Lachenbruch, A.H., DeRito, R.F., 1992, Heat flow and subsurface temperature as evidence for basin-scale groundwater flow, North slope of Alaska: Geological Society of America, v. 104, p. 528-542.

Deming, D., 1993, Regional permeability estimates from investigations of coupled heat and groundwater flow, North Slope of Alaska: Journal of Geophysical Research, v. 98, no. B9, p. 16271-16286.

Faure, G., 1986, The fission track and other raadiation-damage methods of dating, Principles of Isotope Geology, Ch. 20: New York, John Wiley & Sons, p. 341-362.

Gradstein, F., Agterberg, F.P., Ogg, J.G., Hardenbol, J., vanVeen, P., Thierry, J., and Huang, Z., 1994, A mesozoic time scale: Journal of Geophysical Research, v. 99, no. B12, p. 24051-24074.

Harland, W.B., Armstrong, R.L., Cox, A.V., Craig, L.E., Smith, A.G., and Smith D.G., 1989, A geologic time scale: Cambridge, Cambridge University Press, 163 p.

Hitchon, B., 1984, Geothermal gradients, hydrodynamics, and hydrocarbon occurrences, Alberta, Canada: American Association of Petroleum Geologists Bulletin, v. 68, p. 713-743.

Hitchon, B., 1990, Hydrogeology, geopressures, and hydrocarbon occurrences, Beaufort-Mackenzie Basin: Bulletin of Petroleum Geology, v. 38, p. 215-235.

Issler, D.R., and Snowdon, L.R., 1990, Hydrocarbon generation kinetics and thermal modeling, Beaufort-Mackenzie Basin: Bulletin of Canadian Petroleum Geology, v. 38, p. 1-16.

Issler, D.R., 1992, A new approach to shale compaction and stratigraphic restoration, Beaufort-Mackenzie Basin and Mackenzie Corridor, Northern Canada: American Association of Petroleum Geologists Bulletin, v. 76, p. 1170-1189.

Johnsson, M.J., Pawlewicz, M.J., Harris, A.G., and Valin, Z.C, 1992, Vitrinite reflectance and conodant alteration index data from Alaska: U.S. Geological Survey Open-File Report 92-409.

Lachenbruch, A.H., Sass, J.H., Lawver, L.A., Brewer, M.C., Marshall, B.V., Munroe, R.J., Kennelly, J.P., Galanis, S.P., Moses, T.H., 1988, Temperature and depth of permafrost on the Arctic slope of Alaska, in Gryc, G., ed., Geology and Exploration of the National Petroleum Reserve in Alaska, 1974-1982, U.S. Geological Survey Professional Paper 1399, Ch. 28, p. 645-656.

Magoon, L.B., Woodward, P.V., Banet, A.C., Griscom, S.B., Daws, T.A., 1987, Thermal maturity, richness, and type of organic matter of source-rock units, in Bird, K.J., Magoon, L.B., ed., Petroleum Geology of the Northern Part of the Arctic National Wildlife Refuge, Northeastern Alaska, U.S. Geological Survey Bulletin 1778, Ch. 11, p. 127-152.

McSweeney, E., 1993, Constraining the thermal history of the North Slope of Alaska utilizing vitrinite reflectance data: Norman, Oklahoma, University of Oklahoma, 114 p.

O'Sullivan, P.B., Green, P.F., Bergman, S.C., Decker, J., Duddy, I.R., Gleadow, A.J.W., Turner, D.L., 1993, Multiple phases of Tertiary uplift and erosion in the Arctic National Wildlife Refuge, Alaska, revealed by Apatite fission track analysis: American Association of Petroleum Geologists Bulletin, v. 77, p. 359-385.

Phillips, S.L., Ozbek, H., Igbene, A., Litton, G., ed., 1980, Viscosity of NaCl and other solutions up to 350 C and 50 MPa pressures, Lawrence Berkeley Laboratory Report LBL-11586, 71 p.

Phillips, S.L., Igbene, A., Fair, J.A., and Ozbek, H., 1981, A technical databook for geothermal energy utilization: Lawrence Berkeley Laboratory Report LBL-12810, 71 p.

Sweeney, J.J., Burnham, A.K., 1990, Evaluation of a simple model of vitrinite reflectance based on chemical kinetics: American Association of Petroleum Geologists Bulletin, v. 74, p. 1559-1570.

Tissot, B.P., Welte, D.H., 1984, Petrolem Formation and Occurrence (Second ed.): New York, Springer-Verlag, 699 p.

Verweij, H., 1997, Post-Carboniferous hydrogeochemistry of the onshore and offshore Netherlands and its control on the evolution of the petroleum systems, *in* Letourneau, J., Rostron, B., Dahlberg, E., and Reid, H., editors, AAPG Hedberg Research Conference, Applied Hydrogeology in Exploration, Abstracts, Banff, Alberta, Canada, July 27-30, 1997.

FIGURES CAPTIONS

Figure 1. Map showing the 1002 region of the Alaska National Wildlife Refuge (ANWR), the Canning River cross-section, and locations of wells that provided stratigraphic control in the model.

Figure 2. Canning River cross-section; a-i show key 'time slices' in the burial and uplift history of the region.

Figure 3. Cross-section showing approximate locations of AFTA sample sites (A), and locations of nodes where calculations are reported in the Hue Shale (H), and in the Shublik Formation (S).

Figure 4. Burial history calculated for two nodes whose positions approximate the locations of AFT samples (see O'Sullivan et al., 1993, Fig. 4).

Figure 5. Temperature vs. time calculated for two nodes whose positions approximate the locations of AFT samples (see O'Sullivan et al., 1993, Fig. 4). Closure temperatures determined from cooling rates are based on Faure (1986, Fig. 20-2).

Figure 6. Calculated vitrinite reflectance values a) plotted vs. depth and superimposed on measured values for the four southern wells in the Canning River section, b) for the three northern wells in the section, and c) plotted as contours on the cross section. Vitrinite reflectance data are from Bird et al. (in prep.).

Figure 7. Oil generation vs. time in the Shublik Formation a) using the best available kinetic constants and b) using Phosphoria Shale constants (Table 4).

Figure 8. Oil generation vs. time in the Hue Shale a) using the best available kinetic constants and b) using Phosphoria Shale constants (Table 4).

Figure 9. Vitrinite reflectance values vs. time calculated for several locations in the Hue Shale.

Figure 10. Oil generation vs. time for the Mikkelsen Tongue of the Canning Formation using Phosphoria Shale constants. The Mikkelsen Tongue has the deepest burial history at node (30, 17) at the north end of the section.

TABLES CAPTIONS

Table 1. Summary of stratigraphy and formation ages. Ages are based on Berggren et al. (1995), Gradstein et al. (1994); Harland et al. (1989).

Table 2. ANWR model input.

Table 3. Table 3. Physical properties of rocks assumed in ANWR model (modified from Bethke et al., 1993, Table 2.1).

Table 4. Summary of kinetic constants for ANWR and other localities for comparison.

APPENDIX

Basin2 input file for ANWR model.

Appendix

Basin2 Input file for Canning River (ANWR) model

```
#ANWAR: N-S Cross-Section: Canning A-1 Well to Hammerhead-1 Well.
# E. Rowan 8/5/97; saved as B2in.Aug5
#_____________________________________________________________

# *** 9  Wells (South to North):
#(1) Canning River A-1, (2) "Dummy" well, (3) Canning River B-1,
#(4) Beli Unit-1, (5) Alaska J-1, (6) Leffingwell-1,
#(7) West Staines #State-2, (8) Pt. Thomson Unit-1, (9) Hammerhead-1.

#"Dummy" well at 1.52 km "pins" strat. in first column.

#Distances (km) projected onto N-S line of section:
x_well (km) 0.0, 1.52, 6.0, 12.0, 28.0, 46.0, 56.3, 66.25, 84.5
#_____________________________________________________________
temperature = conductive; flow = vertical
nx = 30; width = 90
vitrinite = on; arrhenius = on
compaction = irreversible
left = open; right = open
#_____________________________________________________________
#Kerogen Maturation-Kinetic constants (units: kJ/mol, 1/hours)
#Notes from Paul Lillis. See end of file for more constants.
#act_eng = 224.208;   pre_fac = 2.04e17 #for Shublik
#act_eng = 221.2499;  pre_fac = 1.19e17 #for Hue Shale
#act_eng = 230;              pre_fac = 4.54e17 #for Mikkelson Tongue
#_____________________________________________________________
rock ss
b_tc = .006150; phi0 = 0.20; phi1 = 0.025

rock sh
b_tc = .006150; phi0 = 0.30; phi1 = 0.025

rock cn
b_tc = .006150; phi0 = 0.20; phi1 = 0.025

end_rock
#_____________________________________________________________

strat '(1) Pre-Mississippian basement  (Devonian and older:>362.5 m.y.)'
X(ss) = 1
t_dep = -362.5 m.y.; thickness = 1000 ft; surface_temp = 19.5 C

strat '(2) LMU--Lower Mississippian Unconformity (345-362.5 m.y.)'
t_dep = -345.0 m.y.; thickness = 0; surface_temp = 19.5 C

strat '(3) Endicott Gp. (Middle & Upper Mississippian: 333-345 m.y.)'
#Kayak Shale + Kekiktuk Conglomerate
t_dep = -333 m.y.; X(sh) = .75, X(ss) = .25
surface_temp = 19 C; water_depth = 30 m
column thickness (ft)
w(1:5) 250
w(6)          700
w(7:9) 0

strat '(4) Lisburne Gp. (Upper Miss. and Penn.: 300-333 m.y.)'
t_dep = -300 m.y.; X(sh) = .08, X(ss) = .06, X(cn)= .86
thickness = 2300 ft; surface_temp = 20 C; water_depth = 30 m

strat '(5) PPU--Post-Penn. Unconformity (Early Permian: 269-300 m.y.)'
t_dep = -269 m.y.; surface_temp = 19.5 C; thickness = 0
```

```
strat '(6) Sadlerochit+Shublik+Sag (U. Permian-Triassic: 208-269 m.y.)'
#Sadlerochit Gp.(290-240) + Shublik Fm.+Sag R. Ss (240-208)
t_dep = -208 m.y.; X(sh) = .5; X(ss)=0.5
surface_temp = 19.5 C; water_depth = 30 m
#act_eng = 224.208;   pre_fac = 2.04e17 #for Shublik
act_eng = 178.7;      pre_fac = 4.821e13 #Phosphoria Fm.(for Hue)
column thickness (ft)
w(1)          1315
w(2)          1315
w(3)          1250
w(4)          1190
w(5:9) 1190          #erode to 0

strat '(7) Kingak Shale (Jurassic: 135-208 m.y.)'
t_dep = -135 m.y.; X(sh) = 0.95, x(ss) = 0.05
thickness = 1000 ft; surface_temp = 12 C; water_depth = 150 m

strat '(8) LCU--Lower Cretaceous Unconf. (Early Cret.: 130-135 m.y.)'
t_dep = -130 m.y.; surface_temp = 9.5 C
column thickness (ft)
w(1)          0
w(2)          0
w(3)          &
w(4)          &
w(5)          &
w(6)          -4700          #-(1000+1190+2350+250)=4790
w(7)          -4750          # -(1000+1190+2350+250)=4790
w(8)          -4850          #-(1000+1190+2350+250)=4790
w(9)          -4850

strat '(9) Hue Shale (Cret., pre-Maastricht.: 74-130 m.y.)'
#Hue Shale + Pebble shale + Kemik Sandstone
t_dep = -74 m.y.; X(sh) = 0.95, x(ss) = 0.05
surface_temp = 14 C; water_depth = 1000 m
act_eng = 221.2499;   pre_fac = 1.19e17 #for Hue Shale
#act_eng = 178.7;     pre_fac = 4.821e13 #Phosphoria Fm.
column thickness (ft)  heat_flow
w(1)          1250                  1.5
w(2)          1250                  1.5
w(3)          825                   1.5
w(4)          875                   1.5
w(5)          &                     1.25
w(6)          &                     1.25
w(7)          1175                  1.50
w(8)          690                   1.50
w(9)          690                   1.50

strat '(10) lowermost tongue of Canning Fm (Cretaceous: 65-74 m.y.)'
#Cretaceous, Maastrichtian
t_dep = -65 m.y.; surface_temp = 17 C
X(ss) = 0.19; X(sh) = 0.81; water_depth = 30 m
column thickness (ft)            heat_flow
w(1)          2200                  1.5
w(2)          2200                  1.5
w(3)          1800                  1.5
w(4)          1450                  1.5
w(5)          200                   1.25
w(6)          0                     1.25
w(7)          0                     1.50
w(8)          0                     1.50
w(9)          -700                  1.50

strat '(11) Paleocene--lower Canning & lower Sag. Fms. (55-65 m.y.)'
```

```
t_dep = -55 m.y.; X(sh) = 0.66; X(ss) = 0.34
surface_temp = 8 C; water_depth = 30 m
column          thickness (ft)          heat_flow
w(1)            9250                    1.5
w(2)            9250                    1.5
w(3)            8750                    1.5
w(4)            8100                    1.5
w(5)            7000                    1.25
w(6)            5400                    1.25
w(7)            4300                    1.50
w(8)            4300                    1.50
w(9)            2600                    1.50

strat '(12) Eocene--Mikkelson tongue of Canning Fm (47-55 m.y.)'
t_dep = -47 m.y.; X(sh) = 0.8; X(ss) = 0.2
surface_temp = 8 C; water_depth = 30 m
#act_eng = 230;                         pre_fac = 4.54e17 #Eocene Richards Fm
act_eng = 178.7;                pre_fac = 4.821e13 #Phosphoria Fm.
column          thickness (ft)          heat_flow
w(1)            4500                    1.5
w(2)            4500                    1.5
w(3)            4500                    1.5
w(4)            4500                    1.5
w(5)            4500                    1.25
w(6)            2000                    1.25
w(7)            1850                    1.50
w(8)            1600                    1.50
w(9)            1700                    1.50

strat '(13) Eocene-- Erosion (37-47 m.y.)'
t_dep = -37 m.y.; surface_temp = 7.5 C
X(sh) = 0.8; X(ss) = 0.2
column          thickness (ft)          heat_flow
w(1)            -14950                  1.5
w(2)            -14950                  1.5
w(3)            -4500                   1.5
w(4)            &                       1.5
w(5)            &                       1.25
w(6)            0                       1.25
w(7)            0                       1.50
w(8)            0                       1.50
w(9)            0                       1.50

strat '(14) Eocene--post-Mikkelson tongue (34-37 m.y.)'
t_dep = -34 m.y.; surface_temp = 5 C
X(sh) = 0.6; X(ss) = 0.4
column          thickness (ft)          water_depth (m)         heat_flow
w(1)            0                       0                       1.50
w(2)            0                       0                       1.50
w(3)            0                       0                       1.50
w(4)            &                       0                       1.5
w(5)            1500                    30                      1.25
w(6)            2000                    30                      1.25
w(7)            2000                    30                      1.50
w(8)            2000                    30                      1.50
w(9)            1700                    30                      1.50

strat '(15) Oligocene Sagavanirtok Fm. (32-34 m.y.)'
t_dep = -32 m.y.; surface_temp = 4 C
X(sh) = 0.6; X(ss) = 0.4
column          thickness (ft)          water_depth (m)         heat_flow
w(1)            0                       0                       1.50
w(2)            0                       0                       1.50
w(3)            0                       &                       1.50
```

```
w(4)          &                          &                  1.5
w(5)          2000                       &                  1.25
w(6)          3000                       30                 1.25
w(7)          2800                       30                 1.50
w(8)          2900                       30                 1.50
w(9)          5800                       30                 1.50

strat '(16) Oligocene Erosion (24-32 m.y.)'
t_dep = -24 m.y.; surface_temp = 4 C
X(sh) = 0.6; X(ss) = 0.4
#theta = 1; passes = 0; step_increase = 1.5
column        thickness (ft)        water_depth (m)       heat_flow
w(1)          0                          0                  1.50
w(2)          0                          0                  1.50
w(3)          -3100                      0                  1.50
w(4)          &                          0                  1.5
w(5)          0                          0                  1.25
w(6)          0                          30                 1.25
w(7)          "                          30                 1.50
w(8)          "                          30                 1.50
w(9)          "                          30                 1.50

strat '(17) Miocene + Pliocene sediments (2-24 m.y.)'
t_dep = -1.8 m.y.; surface_temp = 0.5 C
X(sh) = 0.6; X(ss) = 0.4
column thickness (ft)        water_depth (ft)  heat_flow
w(1)          0                          -900               1.50
w(2)          0                          &                  1.50
w(3)          0                          &                  1.50
w(4)          0                          &                  1.5
w(5)          0                          &                  1.25
w(6)          0                          &                  1.25
w(7)          1000                       -65                1.50
w(8)          1700                       -5                 1.50
w(9)          2200                       50                 1.50


strat '(20) Holocene--Form present topog. & water depth (0-2 m.y.)'
t_dep = 0 m.y.; surface_temp = 0.5 C
column  water_depth (ft)     heat_flow
w(1)          900                   1.5
w(2)          &                     1.5
w(3)          &                     1.5
w(4)          &                     1.5
w(5)          &                     1.25
w(6)          &                     1.25
w(7)          -65                   1.50
w(8)          -5                    1.50
w(9)          50                    1.50
end_strat
#_____________________________________________________________
#Kerogen Maturation-Kinetic constants (units: kJ/mol, 1/hours)
#Notes from Paul Lillis
#act_eng = 178.7;     pre_fac = 4.821e13 #Phosphoria Fm.(for Hue)
#act_eng = 201.3;     pre_fac = 1.765e15 #Alum Shale
#act_eng = 269;pre_fac = 8.539e20   #Green R. (slow)
#act_eng = 219;pre_fac = 1.013e17   #Green R.(medium)
#act_eng = 194;pre_fac = 1.153e15   #Green R. (fast)
#act_eng = 218.25;pre_fac = 6.51e16 #Woodford Shale
#_____________________________________________________________

#Add back in future work. Permafrost sections don't work with B2plot.
#Wannt permafrost in order to compare calculated with measured thermal
#profiles in present day.
```

```
#rock ss1
#A_tc = 0 ; B_tc = 0.5

#rock sh1      #High therm. cond. to keep temp const. thru PF.
#A_Perm = 8; B_Perm = -7 log_darcy; phi0 = .55; phi1= .05
#p_kxkz = 10; bpor = 0.85; bpor_ul = 0.17; rho_rk = 2.74
#A_tc = 0; B_tc = 0.5

#strat '(18) EPU--Early Pleistocene Unconf. (1.7-1.65 m.y.)'
##Rapid erosion of 2000' of sediments; replace with permafrost.
#t_dep = -1.65 m.y.; surface_temp = 0.5 C
#X(sh) = 0.6; X(ss) = 0.4
#column        thickness (ft)        water_depth (ft)
#w(1)   -1800   -895  #add topo to check strats bef. pf.
#w(2)   -1800   -895
#w(3)   -1805   -666
#w(4)   -1680   -1022
#w(5)   -1965   &
#w(6)   -1965   &
#w(7)   -1965   -65
#w(8)   -1955   -5
#w(9)   -300    50

#w(4)   -2670   #These values crash b2plot
#w(5)   -2218
#w(6)   -2008

#strat '(19)  Pleistocene (1.65 - 1.6 m.y.)'
##Add back seds as permafrost
#t_dep = -1.6 m.y.; surface_temp = 0.5 C
#X(ss1) = 0.4; X(sh1) = 0.6
#column        thickness (ft)        water_depth (ft)
#w(1)   1800    -895
#w(2)   1800    -895
#w(3)   1805    -666
#w(4)   1680    -1022
#w(5)   1965    &
#w(6)   1965    &
#w(7)   1965    -65
#w(8)   1955    -5
#w(9)   300     50

#w(4)   2670    &
#w(5)   2218    &
#w(6)   2008    0
```

Table 1. Summary of stratigraphy and formation ages. Ages are based on Berggren et al., 1995; Gradstein et al., 1994; Harland et al., 1989. Stratigraphy from Detterman et al., 1975; Bird and Molnaar, 1987.

Group/Fm Member/Unit	Age of Fm. top (era)	(m.y.)	Model Unit No.	Time-stratigraphic unit in model	Interval (m.y.)
Surficial deposits (Holocene)	present	0	20	Holocene: topography	0-2
Gublik Fm (Pleistocene)	Pleistocene				
			19*	Pleistocene: Permafrost formed	
Early Pleistocene Unconformity			18*	Early Pleistocene Unconformity	
upper Sagavanirtok Fm	Tertiary	1.77	17	Miocene + Pliocene: Sagavanirtok Fm.	2-24
uppermost Sag		23.8	16	Oligocene Erosion	24-32
			15	Oligocene: Sagavanirtok Fm.	32-34
upper Canning Fm	Eocene	33.7	14	Eocene-post Mikkelson Tongue: upper Canning Fm	34-37
			13	Eocene Erosion	37-47
			12	Eocene-Mikkelson Tongue: upper Canning Fm	47-55
lower Canning + lower Sagavanirtok	Paleocene	55	11	Paleocene: lower Cann.+lower Sag.	55-65
Staines tng of Sag (pre-Eo)					
unamed tng of Can (upper)					
upper tng of Sag					
unamed tng of Can (middle)					
lower tng of Sag					
lowermost tng of Can (Tert)					
lowermost tongue of Canning (Cret.)	Maastrichtian	65	10	Latest Cret.: lowermost tng. of Canning	65-74
Hue Shale	Campanian	74	9	Cretaceous (pre-Maastrichtian): Hue Shale	74-130
upper portion					
gamma ray zone					
Pebble shale					
Kemik Sandstone					
Lower Cretaceous Unconformity (LCU)	mid-Hauteriveran	130	8	Lower Cretaceous Unconformity	130-135
Kingak Shale**	mid-Valanginian	135	7	Jurassic: Kingak Shale	135-208
Sag R./Karen Cr. Sandstone	Rhaetian	208	6	Upper Permian-Triassic: Sag R.+Shublik Fm.	208-269
Shublik Fm	Norian	209.5		+ SADLEROCHIT GP	
SADLEROCHIT GP	E. Triassic	241.1			
Ivishak Fm					
Fire Cr. Siltstone Mbr	E. Triassic				
Ledge Sandstone Mbr					
Kavik Mbr					
Echooka Fm	U. Permian	245			
Post-Pennsylvanian Unconformity	Sakmarian	269	5	Post-Penn. Unconformity	269-300
LISBURNE GP	Pennsylvanian	300	4	Pennsylvanian: LISBURNE GP	300-333
ENDICOTT GP	M & U Miss.	333	3	Mississippian: ENDICOTT GP	333-345
Kayak Shale	U. Miss				
Kekiktuk Conglomerate					
Lower Mississippian Unconformity	Lower Miss.	345	2	Lower Mississippian Unconformity (LMU)	345-362.5
PRE-MISSISSIPPIAN BASEMENT	Devonian	362.5	1	PRE-MISSISSIPPIAN BASEMENT	>362.5

* These units not included in this version of the ANWR model.

** Age at the top of the Kingak decreases northward.

Abbreviations:

Sag = Sagavanirtok
Can = Canning
Mik = Mikkelson
tng = tongue
GP = Group

Table 2. ANWR model input

Wells: (1) Canning River A-1 (0 km), (2) "Dummy" (1.52 km), (3) Canning River B-1 (6 km), (4) Beli (12 km) , (5) Alaska State J-1 (28 km), (6) Leffingwell (46 km), (7) West Staines-2 (56 km), (8) Point Thompson No. 1 (66 km), (9) Hammerhead No. 1 (84.5 km)

"&" = interpolate value Negative thickness = erosion.

Model Time Interval and Name	Deposition/Erosion (backstripped) (ft)	(km)
Time Interval (1) PRE-MISS. BASEMENT		
>362.5 m.y.		

Time Interval (2) LMU (Lower Mississippian Unconformity)									
345-362.5 m.y.	--Thickness deposited--		---Lithology---			-----Conditions at end of time interval-----			
	ft	km	X(sh)	X(ss)	X(cn)	Water_depth (m)	(ft)	Surface_temp (°C)	Heat flow (HFU)
	0	0.00				0	0	19.5	1.5

Time Interval (3) Mississippian: ENDICOTT GP									
333-345 m.y.	---Thickness deposited---		---Lithology---			----Conditions at end of time interval----			
	ft	km	X(sh)	X(ss)	X(cn)	Water_depth (m)	(ft)	Surface_temp (°C)	Heat flow (HFU)
well (1) A-1	250	0.08	**0.75**	**0.25**		30	99	19	1.5
well (2) A-1	250	0.08	**0.75**	**0.25**		30	99	19	1.5
well (3) B-1	250	0.08	**0.75**	**0.25**		30	99	19	1.5
well (4) Beli	250	0.08	**0.75**	**0.25**		30	99	19	1.5
well (5) J-1	250	0.08	**0.75**	**0.25**		30	99	19	1.5
well (6) Leffingwell	250	0.08	**0.75**	**0.25**		30	99	19	1.5
well (7) W. Staines-2	700	0.21	**0.75**	**0.25**		30	99	19	1.5
well (8) Pt. Thomp.-1	0	0.00	**0.75**	**0.25**		30	99	19	1.5
well (9) Hammerhead-1	0	0.00	**0.75**	**0.25**		30	99	19	1.5

Time Interval (4) Upper Mississippian and Pennsylvanian: LISBURNE GP									
300-333 m.y.	---Thickness deposited---		---Lithology---			----Conditions at end of time interval----			
	ft	km	X(sh)	X(ss)	X(cn)	Water_depth (m)	(ft)	Surface_temp (°C)	Heat flow (HFU)
well (1) A-1	2300	0.70	**0.08**	**0.06**	**0.86**	30	99	20	1.5

well (2) A-1	2300	0.70	**0.08**	**0.06**	**0.86**	30	99	20	1.5
well (3) B-1	2300	0.70	**0.08**	**0.06**	**0.86**	30	99	20	1.5
well (4) Beli	2300	0.70	**0.08**	**0.06**	**0.86**	30	99	20	1.5
well (5) J-1	2300	0.70	**0.08**	**0.06**	**0.86**	30	99	20	1.5
well (6) Leffingwell	2300	0.70	**0.08**	**0.06**	**0.86**	30	99	20	1.5
well (7) W. Staines-2	2300	0.70	**0.08**	**0.06**	**0.86**	30	99	20	1.5
well (8) Pt. Thomp.-1	2300	0.70	**0.08**	**0.06**	**0.86**	30	99	20	1.5
well (9) Hammerhead-1	2300	0.70	**0.08**	**0.06**	**0.86**	30	99	20	1.5

Time Interval (5) PPU (Post Pennsylvanian unconformity)

269-300 m.y.	---Thickness deposited---		---Lithology---			----Conditions at end of time interval----			
	ft	km	**X(sh)**	**X(ss)**	**X(cn)**	Water_depth (m)	(ft)	Surface_temp (°C)	Heat flow (HFU)
	0	0				0	0	19.5	1.5

Time Interval (6)Upper Permian-Triassic: Sag R.+Shublik Fm.+SADLEROCHIT GP

208-269 m.y.	---Thickness deposited---		---Lithology---			----Conditions at end of time interval----			
	ft	km	**X(sh)**	**X(ss)**	**X(cn)**	Water_depth (m)	(ft)	Surface_temp (°C)	Heat flow (HFU)
well (1) A-1	1315	0.40	**0.5**	**0.5**		30	99	19.5	1.5
well (2) A-1	1315	0.40	**0.5**	**0.5**		30	99	19.5	1.5
well (3) B-1	1250	0.38	**0.5**	**0.5**		30	99	19.5	1.5
well (4) Beli	1190	0.36	**0.5**	**0.5**		30	99	19.5	1.5
well (5) J-1	1190	0.36	**0.5**	**0.5**		30	99	19.5	1.5
well (6) Leffingwell	1190	0.36	**0.5**	**0.5**		30	99	19.5	1.5
well (7) W. Staines-2	1190	0.36	**0.5**	**0.5**		30	99	19.5	1.5
well (8) Pt. Thomp.-1	1190	0.36	**0.5**	**0.5**		30	99	19.5	1.5
well (9) Hammerhead-1	1190	0.36	**0.5**	**0.5**		30	99	19.5	1.5

Time Interval (7) Early Cretaceous and Jurassic: Kingak Shale

135-208 m.y.	---Thickness deposited---		---Lithology---			----Conditions at end of time interval----			
	ft	km	**X(sh)**	**X(ss)**	**X(cn)**	Water_depth (m)	(ft)	Surface_temp (°C)	Heat flow (HFU)
well (1) A-1	1000	0.30	**0.95**	**0.05**		150	495	12	1.5
well (2) A-1	1000	0.30	**0.95**	**0.05**		150	495	12	1.5
well (3) B-1	1000	0.30	**0.95**	**0.05**		150	495	12	1.5
well (4) Beli	1000	0.30	**0.95**	**0.05**		150	495	12	1.5
well (5) J-1	1000	0.30	**0.95**	**0.05**		150	495	12	1.5
well (6) Leffingwell	1000	0.30	**0.95**	**0.05**		150	495	12	1.5

well (7) W. Staines-2	1000	0.30	**0.95**	**0.05**	150	495	12	1.5
well (8) Pt. Thomp.-1	1000	0.30	**0.95**	**0.05**	150	495	12	1.5
well (9) Hammerhead-1	1000	0.30	**0.95**	**0.05**	150	495	12	1.5

Time Interval (8) LCU									
130-135 m.y.	---Thickness deposited---		---Lithology---			----Conditions at end of time interval----			
	ft	km	**X(sh)**	**X(ss)**	**X(cn)**	Water_depth (m)	(ft)	Surface_temp (°C)	Heat flow (HFU)
well (1) A-1	0	0.00				0	0	9.5	1.5
well (2) A-1	0	0.00				0	0	9.5	1.5
well (3) B-1	&	&				0	0	9.5	1.5
well (4) Beli	&	&				0	0	9.5	1.5
well (5) J-1	&	&				0	0	9.5	1.5
well (6) Leffingwell	-4700	-1.42				0	0	9.5	1.5
well (7) W. Staines-2	-4750	-1.44				0	0	9.5	1.5
well (8) Pt. Thomp.-1	-4850	-1.47				0	0	9.5	1.5
well (9) Hammerhead-1	-4850	-1.47				0	0	9.5	1.5

Time Interval (9) Cret. (pr Hue Sh + Pebble Sh + Kemik SS									
74-130 m.y.	---Thickness deposited---		---Lithology---			----Conditions at end of time interval----			
	ft	km	**X sh)**	**X(ss)**	**X(cn)**	Water_depth m)	(ft)	Surface_temp (°C)	Heat flow (HFU)
well (1) A-1	1250	0.38	**0.95**	**0.05**		1000	3300	14	1.5
well (2) A-1	1250	0.38	**0.95**	**0.05**		1000	3300	14	1.5
well (3) B-1	825	0.25	**0.95**	**0.05**		1000	3300	14	1.5
well (4) Beli	875	0.27	**0.95**	**0.05**		1000	3300	14	1.5
well (5) J-1	&	&	**0.95**	**0.05**		1000	3300	14	1.25
well (6) Leffingwell	&	&	**0.95**	**0.05**		1000	3300	14	1.25
well (7) W. Staines-2	1175	0.36	**0.95**	**0.05**		1000	3300	14	1.5
well (8) Pt. Thomp.-1	690	0.21	**0.95**	**0.05**		1000	3300	14	1.5
well (9) Hammerhead-1	690	0.21	**0.95**	**0.05**		1000	3300	14	1.5

Time Interval (10) Latest Cret. (to T-C boundary): lowermost tng. of Canning									
65-74 m.y.	---Thickness deposited---		---Lithology---			----Conditions at end of time interval----			
	ft	km	**X(sh)**	**X(ss)**	**X(cn)**	Water_depth (m)	(ft)	Surface_temp (°C)	Heat flow (HFU)
well (1) A-1	2200	0.67	**0.81**	**0.19**		30	99	17	1.5
well (2) A-1	2200	0.67	**0.81**	**0.19**		30	99	17	1.5
well (3) B-1	1800	0.55	**0.81**	**0.19**		30	99	17	1.5

well (4) Beli	1450	0.44	**0.81**	**0.19**	30	99	17	1.5
well (5) J-1	200	0.06	**0.81**	**0.19**	30	99	17	1.25
well (6) Leffingwell	0	0.00	**0.81**	**0.19**	30	99	17	1.25
well (7) W. Staines-2	0	0.00	**0.81**	**0.19**	30	99	17	1.5
well (8) Pt. Thomp.-1	0	0.00	**0.81**	**0.19**	30	99	17	1.5
well (9) Hammerhead-1	-700	-0.21	**0.81**	**0.19**	30	99	17	1.5

Time Interval (11) Paleocene: lower Cann.+lower Sag.

55-65 m.y.	---Thickness deposited---		---Lithology---			----Conditions at end of time interval----			
	ft	km	X(sh)	X(ss)	X(cn)	Water_depth (m)	(ft)	Surface_temp (°C)	Heat flow (HFU)
well (1) A-1	9250	2.80	**0.66**	**0.34**		30	99	8	1.5
well (2) A-1	9250	2.80	**0.66**	**0.34**		30	99	8	1.5
well (3) B-1	8750	2.65	**0.66**	**0.34**		30	99	8	1.5
well (4) Beli	8100	2.45	**0.66**	**0.34**		30	99	8	1.5
well (5) J-1	7000	2.12	**0.66**	**0.34**		30	99	8	1.25
well (6) Leffingwell	5400	1.64	**0.66**	**0.34**		30	99	8	1.25
well (7) W. Staines-2	4300	1.30	**0.66**	**0.34**		30	99	8	1.5
well (8) Pt. Thomp.-1	4300	1.30	**0.66**	**0.34**		30	99	8	1.5
well (9) Hammerhead-1	2600	0.79	**0.81**	**0.19**		30	99	8	1.5

Time Interval (12) Eocene-Mikkelson Tongue (upper Canning Fm)

47-55 m.y.	---Thickness deposited---		---Lithology---			----Conditions at end of time interval----			
	ft	km	X(sh)	X(ss)	X(cn)	Water_depth (m)	(ft)	Surface_temp (°C)	Heat flow (HFU)
well (1) A-1	4500	1.36	**0.8**	**0.2**		30	99	8	1.5
well (2) A-1	4500	1.36	**0.8**	**0.2**		30	99	8	1.5
well (3) B-1	4500	1.36	**0.8**	**0.2**		30	99	8	1.5
well (4) Beli	4500	1.36	**0.8**	**0.2**		30	99	8	1.5
well (5) J-1	4500	1.36	**0.8**	**0.2**		30	99	8	1.25
well (6) Leffingwell	2000	0.61	**0.8**	**0.2**		30	99	8	1.25
well (7) W. Staines-2	1850	0.56	**0.8**	**0.2**		30	99	8	1.5
well (8) Pt. Thomp.-1	1600	0.48	**0.8**	**0.2**		30	99	8	1.5
well (9) Hammerhead-1	1700	0.52	**0.8**	**0.2**		30	99	8	1.5

Time Interval (13) Eocene Erosion

37-47 m.y.	---Thickness deposited---		---Lithology---			----Conditions at end of time interval----			
	ft	km	X(sh)	X(ss)	X(cn)	Water_depth (m)	(ft)	Surface_temp (°C)	Heat flow (HFU)

well (1) A-1	-14950	-4.53		0	0	7.5	1.5
well (2) A-1	-14950	-4.53		0	0	7.5	1.5
well (3) B-1	-4500	-1.36		0	0	7.5	1.5
well (4) Beli	&	&		0	0	7.5	1.5
well (5) J-1	&	&		0	0	7.5	1.25
well (6) Leffingwell	0	0.00		0	0	7.5	1.25
well (7) W. Staines-2	0	0.00		0	0	7.5	1.5
well (8) Pt. Thomp.-1	0	0.00		0	0	7.5	1.5
well (9) Hammerhead-1	0	0.00		0	0	7.5	1.5

Time Interval (14) Eocene-post Mikkelson Tongue: upper Canning Fm

34-37 m.y.	---Thickness deposited---		---Lithology---			----Conditions at end of time interval----			
	ft	km	X(sh)	X(ss)	X(cn)	Water_depth (m)	(ft)	Surface_temp (°C)	Heat flow (HFU)
well (1) A-1	0	0.00	**0.6**	**0.4**		0	0	5	1.5
well (2) A-1	0	0.00	**0.6**	**0.4**		0	0	5	1.5
well (3) B-1	0	0.00	**0.6**	**0.4**		0	&	5	1.5
well (4) Beli	&	&	**0.6**	**0.4**		0	&	5	1.5
well (5) J-1	1500	0.45	**0.6**	**0.4**		30	&	5	1.25
well (6) Leffingwell	2000	0.61	**0.6**	**0.4**		30	99	5	1.25
well (7) W. Staines-2	2000	0.61	**0.6**	**0.4**		30	99	5	1.5
well (8) Pt. Thomp.-1	2000	0.61	**0.6**	**0.4**		30	99	5	1.5
well (9) Hammerhead-1	1700	0.52	**0.6**	**0.4**		30	99	5	1.5

Time Interval (15) Oligocene: Sagavanirtok Fm.

32-34 m.y.	---Thickness deposited---		---Lithology---			----Conditions at end of time interval----			
	ft	km	X(sh)	X(ss)	X(cn)	Water_depth (m)	(ft)	Surface_temp (°C)	Heat flow (HFU)
well (1) A-1	0	0.00	**0.6**	**0.4**		0	0	4	1.5
well (2) A-1	0	0.00	**0.6**	**0.4**		0	0	4	1.5
well (3) B-1	0	0.00	**0.6**	**0.4**		&	&	4	1.5
well (4) Beli	&	&	**0.6**	**0.4**		&	&	4	1.5
well (5) J-1	2000	0.61	**0.6**	**0.4**		&	&	4	1.25
well (6) Leffingwell	3000	0.91	**0.6**	**0.4**		30	99	4	1.25
well (7) W. Staines-2	2800	0.85	**0.6**	**0.4**		30	99	4	1.5
well (8) Pt. Thomp.-1	2900	0.88	**0.6**	**0.4**		30	99	4	1.5

well (9) Hammerhead-1	5800	1.76	**0.6**	**0.4**		30	99	4	1.5

Time Interval (16) Oligocene Erosion									
24-32 m.y.	---Thickness deposited---		---Lithology---			----Conditions at end of time interval----			
	ft	km	**X(sh)**	**X(ss)**	**X(cn)**	Water_depth (m)	(ft)	Surface_temp (°C)	Heat flow (HFU)
well (1) A-1	0	0.00				0	0	4	1.5
well (2) A-1	0	0.00				0	0	4	1.5
well (3) B-1	-3100	-0.94				0	0	4	1.5
well (4) Beli	&	&				0	0	4	1.5
well (5) J-1	0	0.00				0	0	4	1.25
well (6) Leffingwell	0	0.00				30	99	4	1.25
well (7) W. Staines-2	0	0.00				30	99	4	1.5
well (8) Pt. Thomp.-1	0	0.00				30	99	4	1.5
well (9) Hammerhead-1	0	0.00				30	99	4	1.5

Time Interval (17) Miocene + Pliocene: Sagavanirtok Fm.									
2-24 m.y.	---Thickness deposited---		---Lithology---			----Conditions at end of time interval----			
	ft	km	**X(sh)**	**X(ss)**	**X(cn)**	Water_depth (m)	(ft)	Surface_temp (°C)	Heat flow (HFU)
well (1) A-1	0	0.00	**0.6**	**0.4**		0	0	0.5	1.5
well (2) A-1	0	0.00	**0.6**	**0.4**		0	0	0.5	1.5
well (3) B-1	0	0.00	**0.6**	**0.4**		0	0	0.5	1.5
well (4) Beli	&	&	**0.6**	**0.4**		0	0	0.5	1.5
well (5) J-1	1500	0.45	**0.6**	**0.4**		30	99	0.5	1.25
well (6) Leffingwell	2000	0.61	**0.6**	**0.4**		30	99	0.5	1.25
well (7) W. Staines-2	2000	0.61	**0.6**	**0.4**		30	99	0.5	1.5
well (8) Pt. Thomp.-1	2000	0.61	**0.6**	**0.4**		30	99	0.5	1.5
well (9) Hammerhead-1	1700	0.52	**0.6**	**0.4**		30	99	0.5	1.5

Time Interval (18) EPU: Rapid erosion -- For future work. Not included in model.									
1.8-2 m.y.	---Thickness deposited---		---Lithology---			----Conditions at end of time interval----			
	ft	km	**X(sh)**	**X(ss)**	**X(cn)**	Water_depth (m)	(ft)	Surface_temp (°C)	Heat flow (HFU)
well (1) A-1	0	0.00				0	0	0.5	1.5
well (2) A-1	0	0.00				0	0	0.5	1.5
well (3) B-1	0	0.00				0	0	0.5	1.5
well (4) Beli	0	0.00				0	0	0.5	1.5
well (5) J-1	&	&				0	0	0.5	1.25

well (6) Leffingwell	-2000	-0.61				0	0	0.5	1.25
well (7) W. Staines-2	&	&				0	0	0.5	1.5
well (8) Pt. Thomp.-1	&	&				0	0	0.5	1.5
well (9) Hammerhead-1	0	0.00				0	0	0.5	1.5

Time Interval (19) Pleistocene: Permafrost -- For future work. Not included in model.

1.75-1.8 m.y.	---Thickness deposited---		---Lithology---			----Conditions at end of time interval----			
	ft	km	X(sh)	X(ss)	X(cn)	Water_depth (m)	(ft)	Surface_temp (°C)	Heat flow (HFU)
well (1) A-1	0	0.00				-300	-990	0.5	1.5
well (2) A-1	0	0.00				-300	-990	0.5	1.5
well (3) B-1	0	0.00				&	&	0.5	1.5
well (4) Beli	0	0.00	1			&	&	0.5	1.5
well (5) J-1	&	&	1			&	&	0.5	1.25
well (6) Leffingwell	2000	0.61	1			&	&	0.5	1.25
well (7) W. Staines-2	&	&	1			0	0	0.5	1.5
well (8) Pt. Thomp.-1	&	&	1			0	0	0.5	1.5
well (9) Hammerhead-1	0	0.00	1			0	0	0.5	1.5

Time Interval (20) Holocene

0-2 m.y.	---Thickness deposited---		---Lithology---			Top of time interval ----Conditions at end of time interval----			
	ft	km	X(sh)	X(ss)	X(cn)	Water_depth (m)	(ft)	Surface_temp (°C)	Heat flow (HFU)
well (1) A-1	0	0.00				-271	-895	0.5	1.5
well (2) A-1	0	0.00				-271	-895	0.5	1.5
well (3) B-1	0	0.00				-202	-666	0.5	1.5
well (4) Beli	0	0.00				-310	-1022	0.5	1.5
well (5) J-1	0	0.00				&	&	0.5	1.25
well (6) Leffingwell	0	0.00				&	&	0.5	1.25
well (7) W. Staines-2	0	0.00				-20	-65	0.5	1.5
well (8) Pt. Thomp.-1	0	0.00				-2	-5	0.5	1.5
well (9) Hammerhead-1	0	0.00				-2	-5	0.5	1.5

Abbreviations:

Sag	Sagavanirtok
Can	Canning
Mik	Mikkelson
tng	tongue
GP	Group

Stratigraphy from Detterman et al., 1975; Bird and Molnaar, 1987.

Table 3. Physical properties of rocks assumed in ANWR model (modified from Bethke et al., 1993, Table 2.1)

Porosity	Variable name (Basin2)	Units	Sandstone	Shale	Carbonate
Reducible porosity present at deposition	ϕ_0, phi0		0.2	0.3	0.2
Irreducible porosity	ϕ_1, phi1		0.025	0.025	0.025
Exponential coefficient describing compaction	b, bpor	(1/km)	0.5	0.85	0.55
Exponential coefficient for rebound during unloading	b_{ul}, bpor_ul	(1/km)	0.1	0.17	0.11
Permeability					
Slope of permeability correlation with porosity	A_perm	(log darcy)	15	8	6
Intercept of permeability correlation with porosity	B_perm	(log darcy)	-3	-7	-4
Anisotropy in permeability	k_x/k_z, p_kxkz		2.5	10	2.5
Thermal conductivity					
Slope of thermal conductivity correlation with porosity	A_tc	(J/m s K) (cal/cm sec°C)	-1.84 -0.0044	-1.84 -0.0044	-1.84 -0.0044
Intercept of thermal conductivity correlation with porosity	B_tc	(J/m s K) (cal/cm sec°C)	2.57 0.0062	2.57 0.0062	2.24 0.00535
Thermal conductivity of water		(J/m s K)	0.60		
Thermal conductivity of bulk medium at 10% porosity (arith. avg.)		(J/m s K)	2.39	2.39	2.06
Grain Density					
Average density of rock (mineral grains)	ρ, rho_rk	(gm/cm3)	2.65	2.74	2.75

Table 4. Summary of kinetic constants for ANWR and other localities for comparison

Name	Ea (kJ/mol)	Ea (kcal/mol)	Ao (1/m.y.)	Ao (1/hr)	Ao (1/s)	Notes
			ANWR (1002) region source rocks			
Hue Shale	221.250	52.845	1.040E+27	1.187E+17	3.30E+13	2
Shublik Fm.	224.208	53.551	1.790E+27	2.043E+17	5.68E+13	2
Mikkelson Tongue	230.000	54.935	3.974E+27	4.536E+17	1.26E+14	7
			Other petroleum source rocks			
Phosphoria Retort Shale	178.69	42.68	4.31E+23	4.92E+13	1.37E+10	1
Phosphoria Retort Shale	178.70	42.68	4.22E+23	4.82E+13	1.34E+10	2
Green River Fm-fast	194.00	46.34	1.01E+25	1.15E+15	3.20E+11	2
Alum Shale	201.30	48.08	1.55E+25	1.77E+15	4.90E+11	2
Woodford Shale	218.25	52.13	5.70E+26	6.51E+16	1.81E+13	1
Green River Fm-medium	219.00	52.31	8.87E+26	1.01E+17	2.81E+13	2
Mahakam Delta	225.94	53.96	3.47E+27	3.96E+17	1.10E+14	3
Eocene Richards Fm.	230.000	54.935	3.974E+27	4.536E+17	1.26E+14	6
San Juan Basin Coal	233.20	55.70	1.28E+28	1.46E+18	4.06E+14	4
Mahakam Delta	247.86	59.20	8.87E+26	1.08E+19	3.00E+15	1, 5
Green River Fm-slow	269.00	64.25	7.48E+30	8.54E+20	2.37E+17	2

1 Joule x .238846 = 1 calorie 1 calorie x 4.1868 = 1 Joule

Notes and references:

1) Lewan (1985)
2) Lillis (pers. comm.)
3) Tissot et al. (1987)
4) Reynolds & Burnham (1992)
5) Behar et al., ms. in prep.
6) Snowdon & Issler (1990)
7) Use values for Eocene Richards Fm.

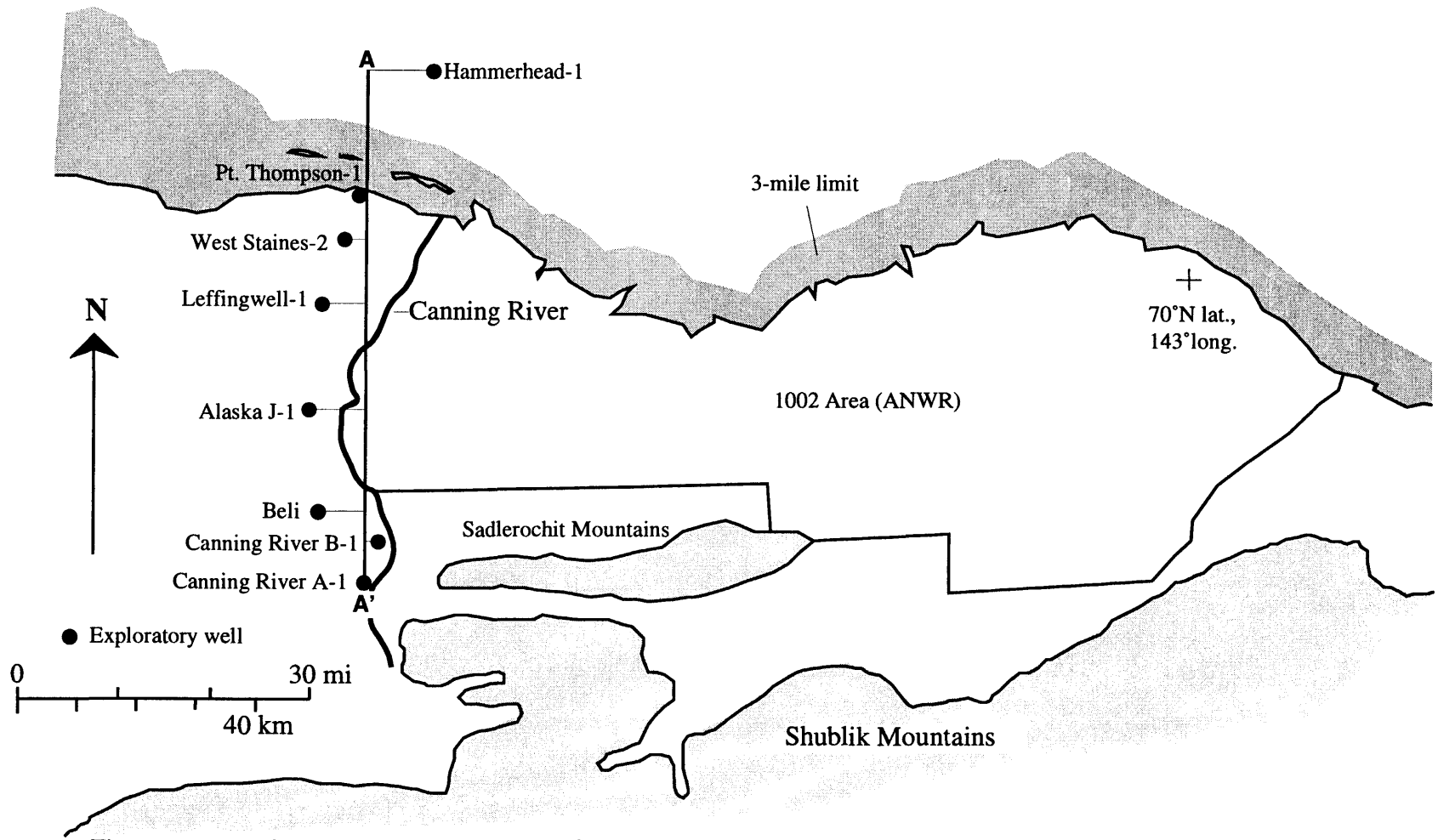

Figure 1. Map showing the 1002 region of the Alaska National Wildlife Refuge (ANWR), the Canning River cross-section (A-A'), and locations of wells that provided stratigraphic control in the model (solid dots). Table 2 provides further information on the wells.

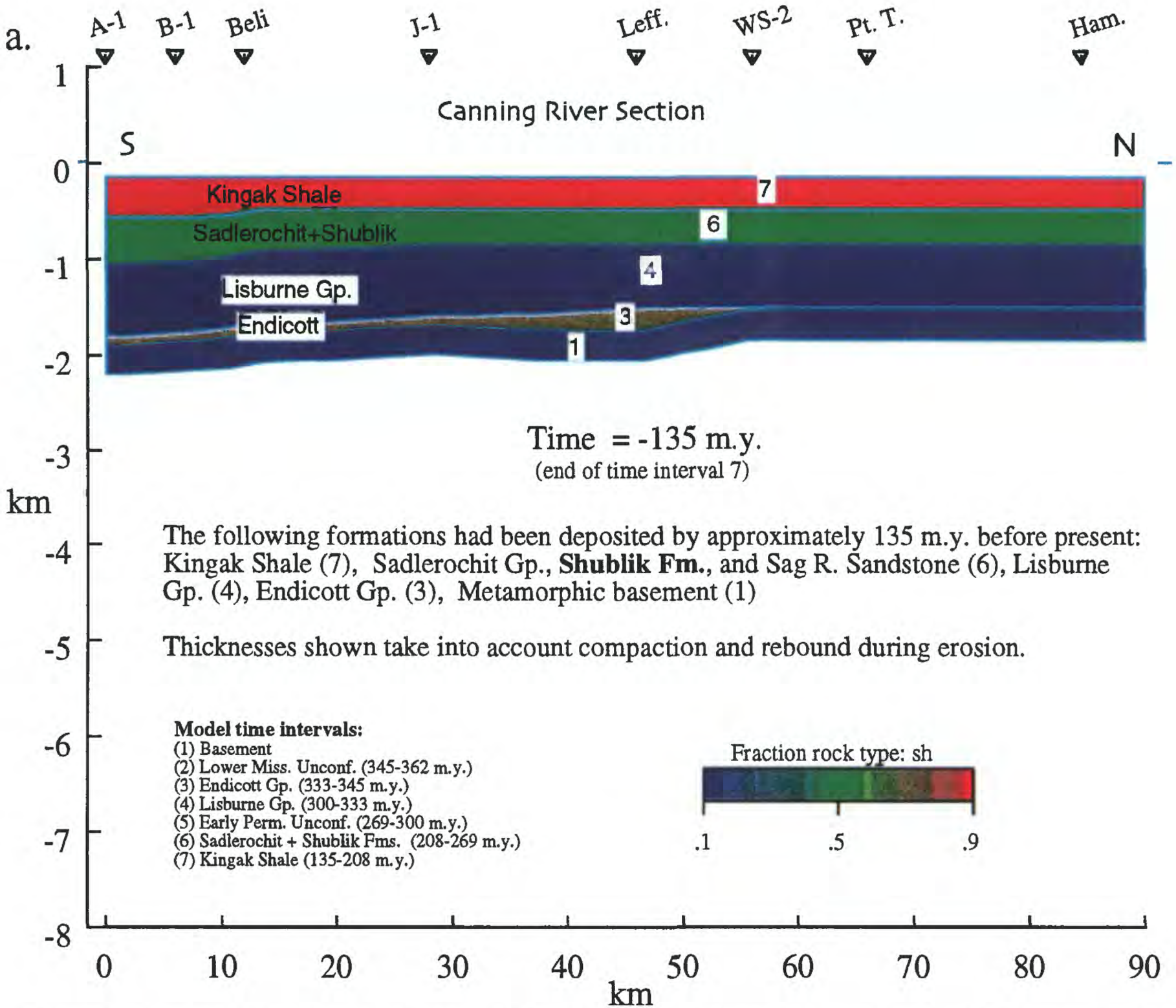

Figure 2. Canning River cross-section; a-i show key 'time slices' in the burial and uplift history of the region.

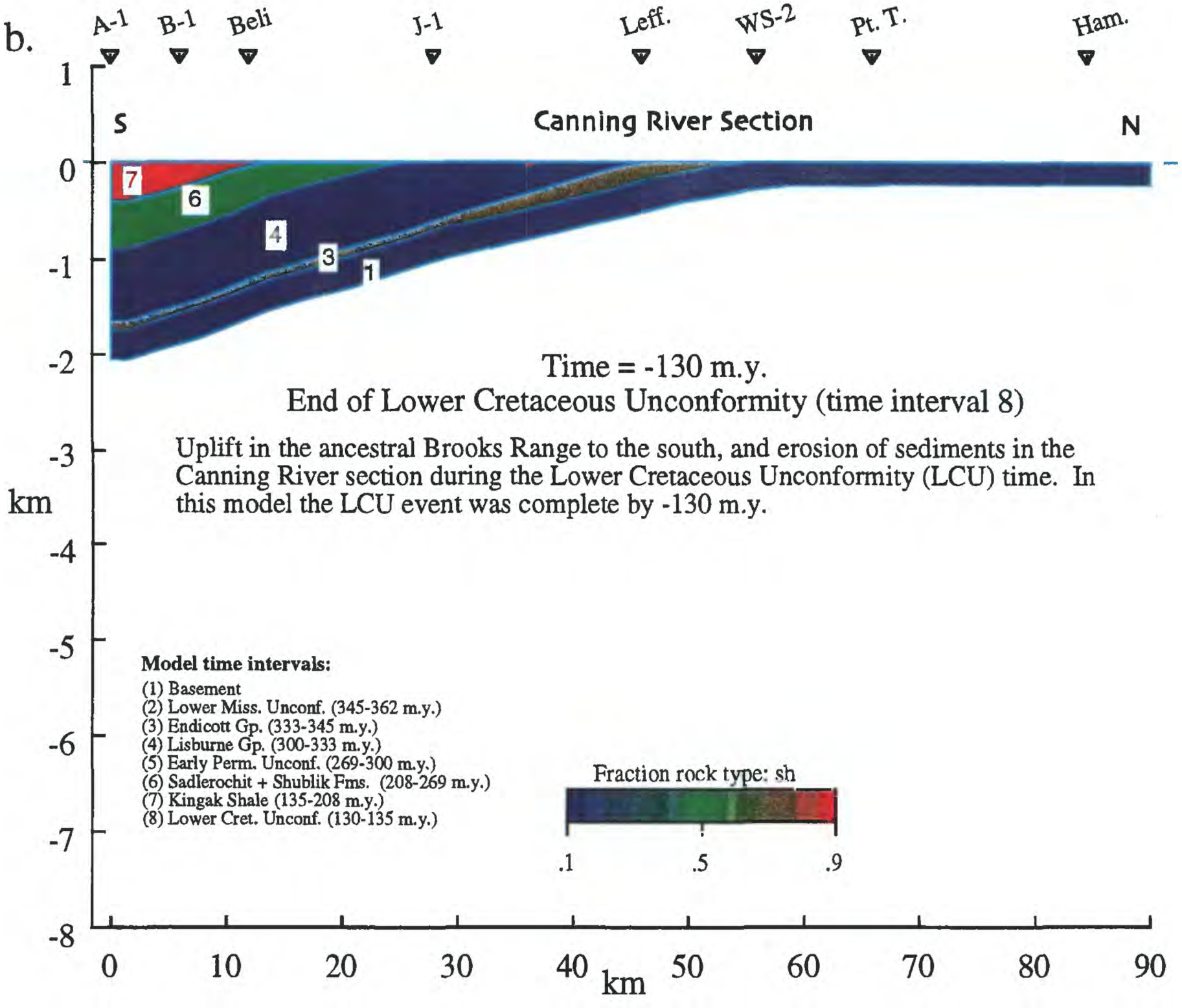

Figure 2. Canning River cross-section; a-i show key 'time slices' in the burial and uplift history of the region.

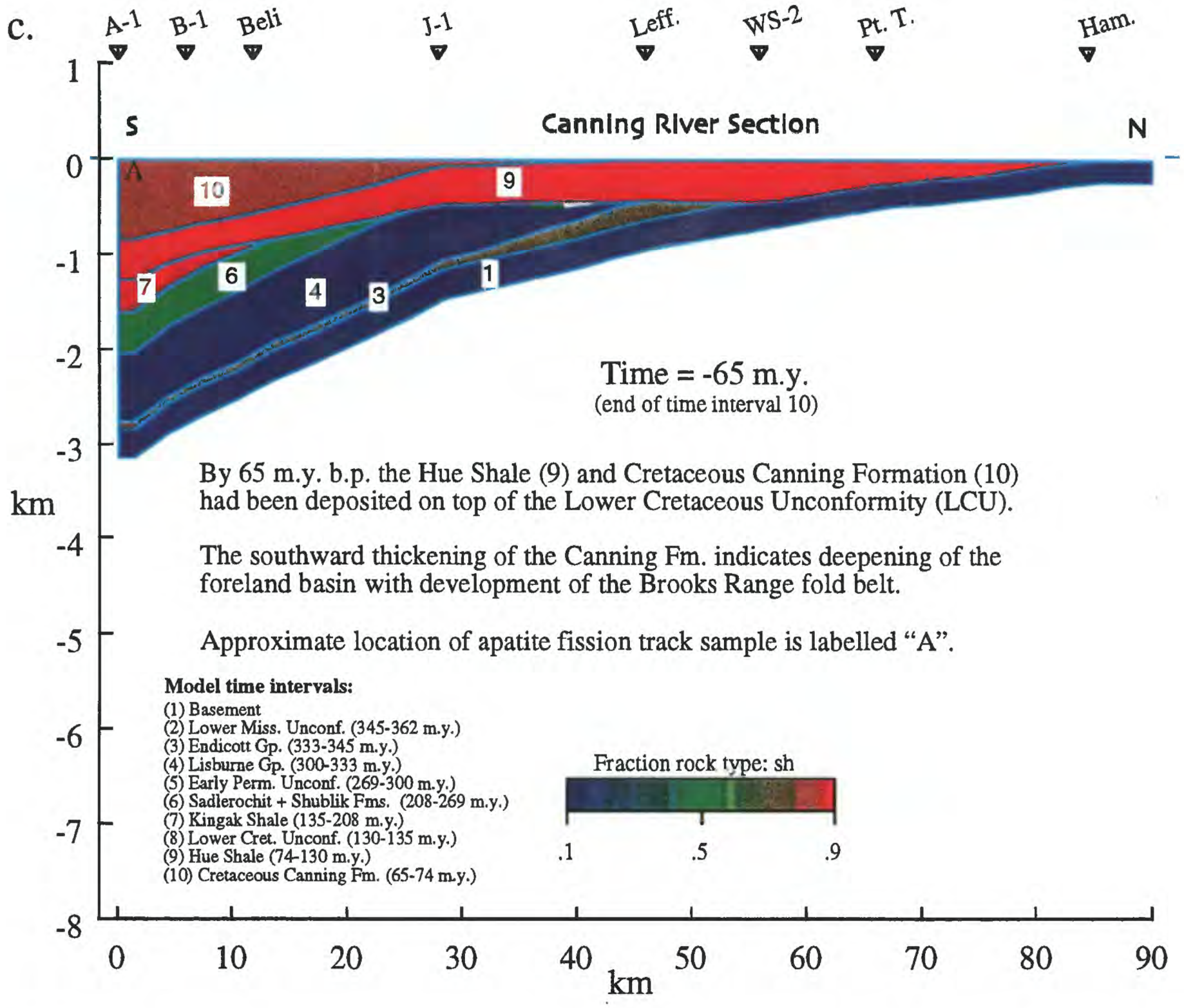

Figure 2. Canning River cross-section; a-i show key 'time slices' in the burial and uplift history of the region.

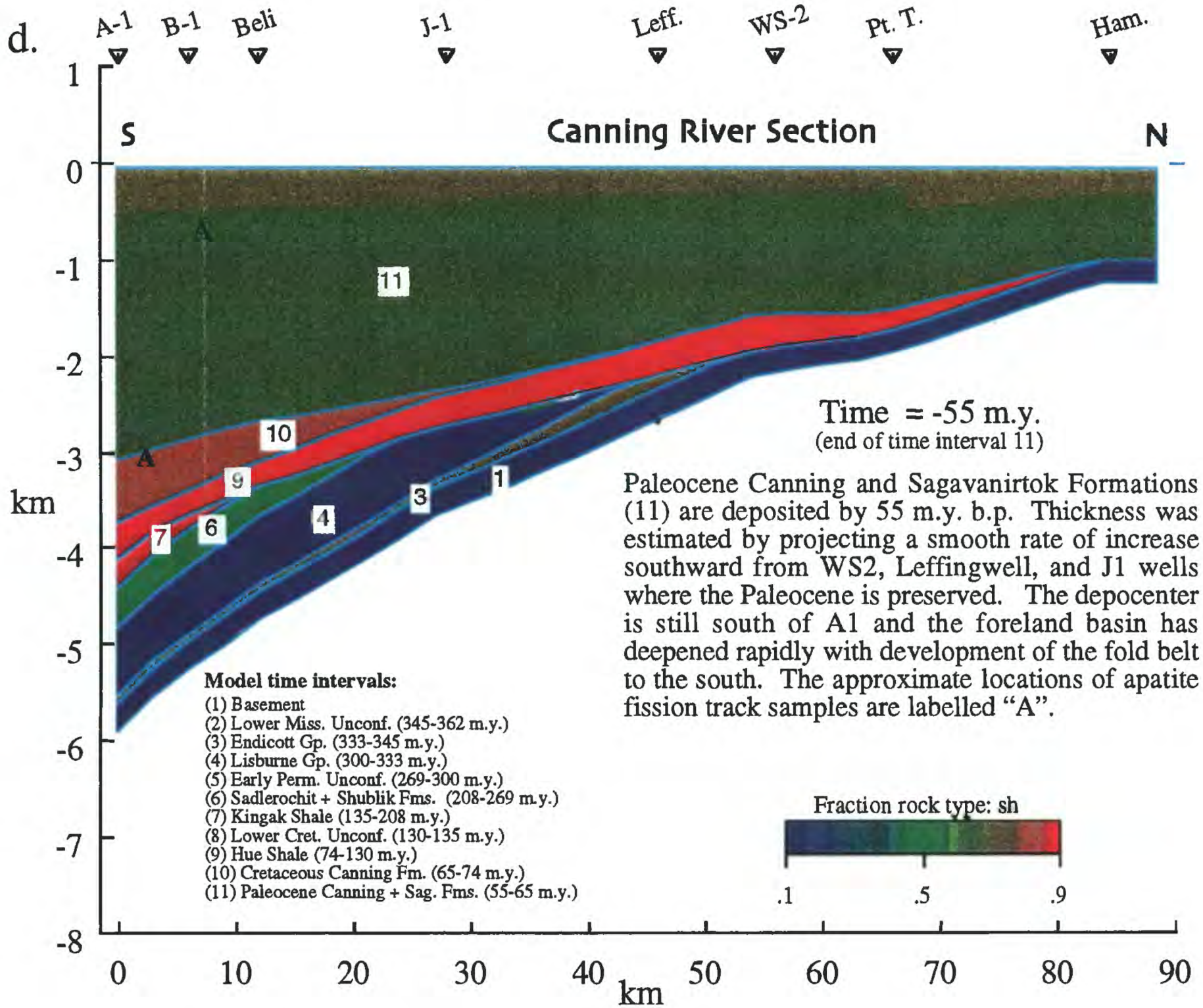

Figure 2. Canning River cross-section; a-i show key 'time slices' in the burial and uplift history of the region.

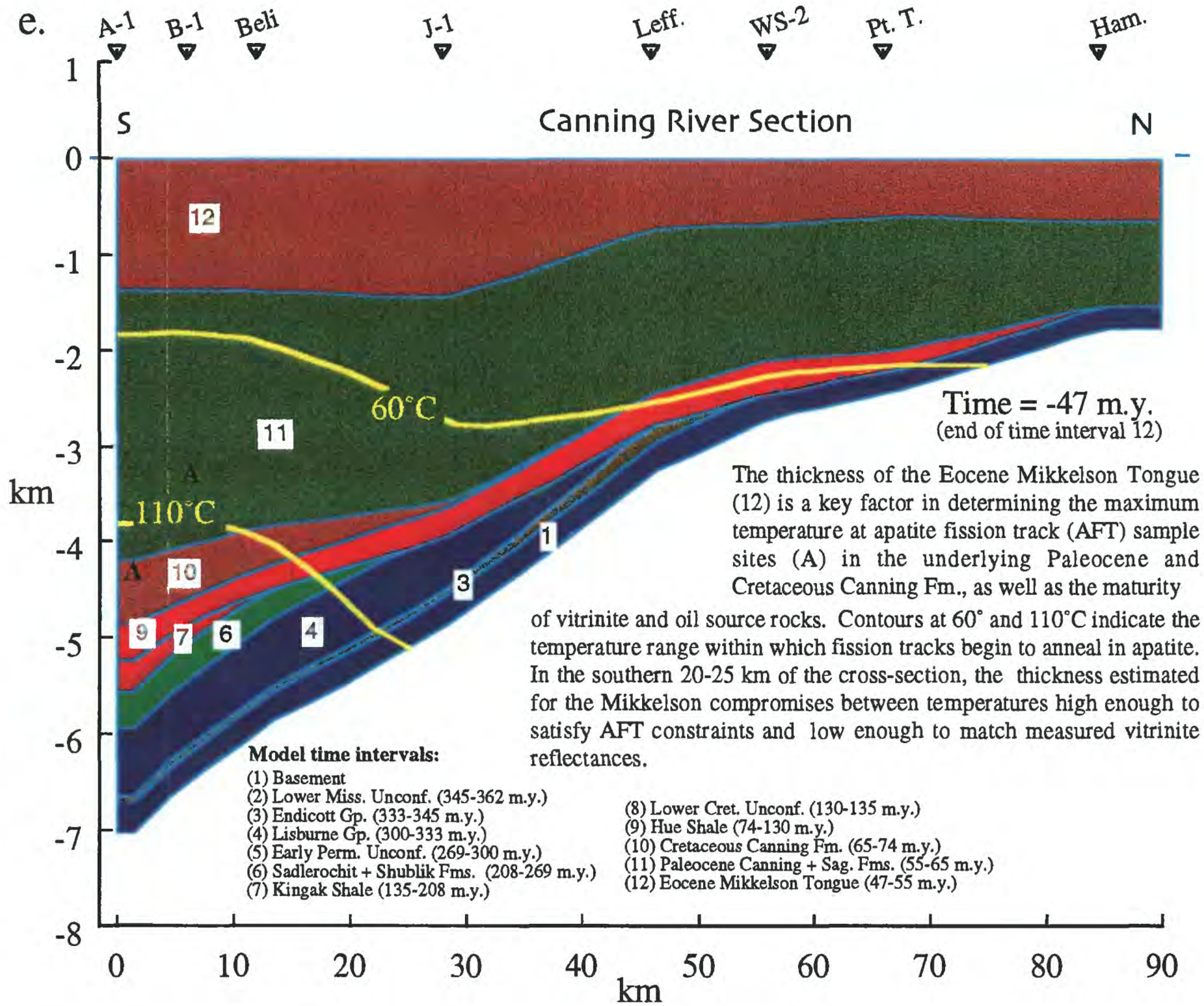

Figure 2. Canning River cross-section; a-i show key 'time slices' in the burial and uplift history of the region.

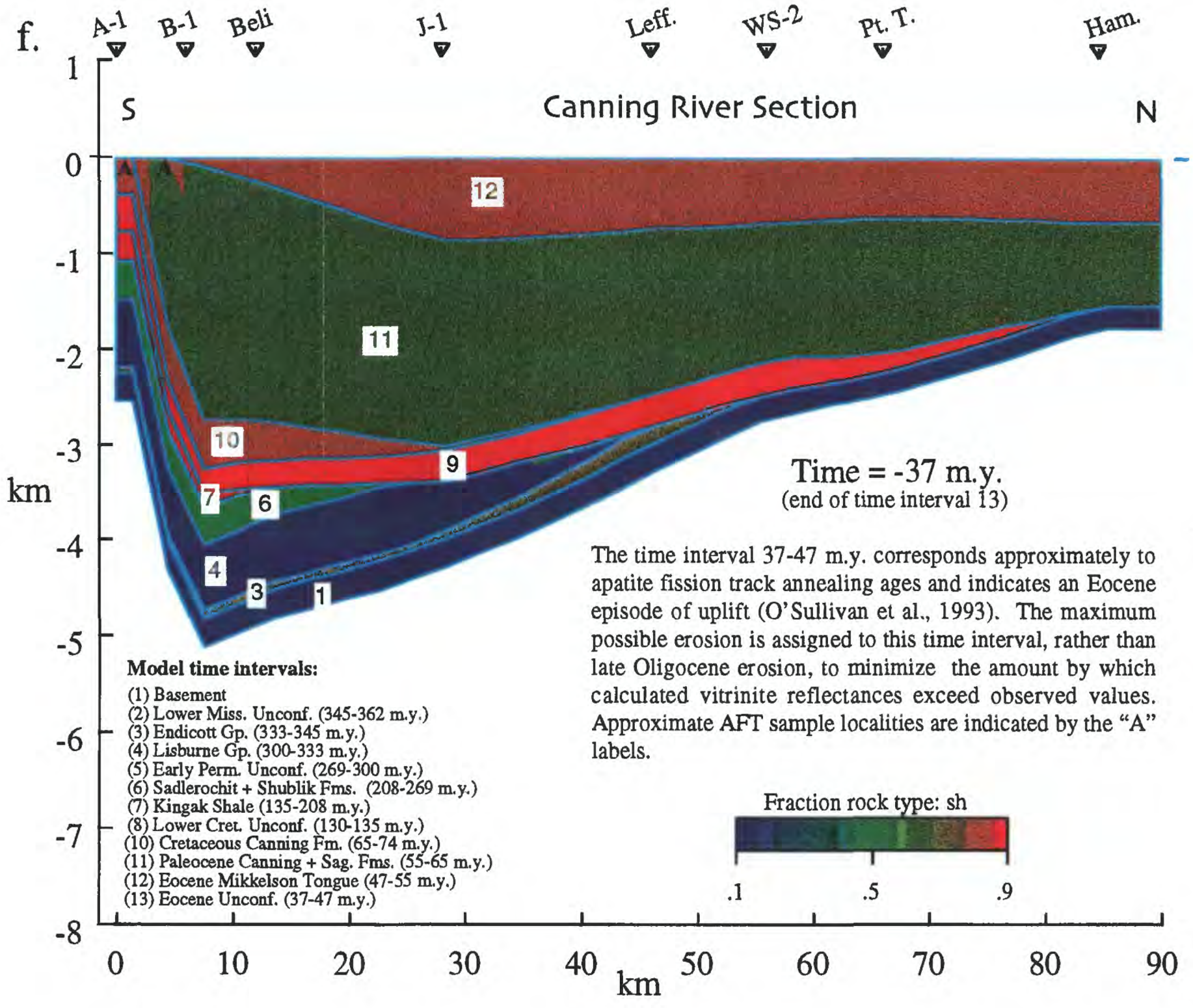

Figure 2. Canning River cross-section; a-i show key 'time slices' in the burial and uplift history of the region.

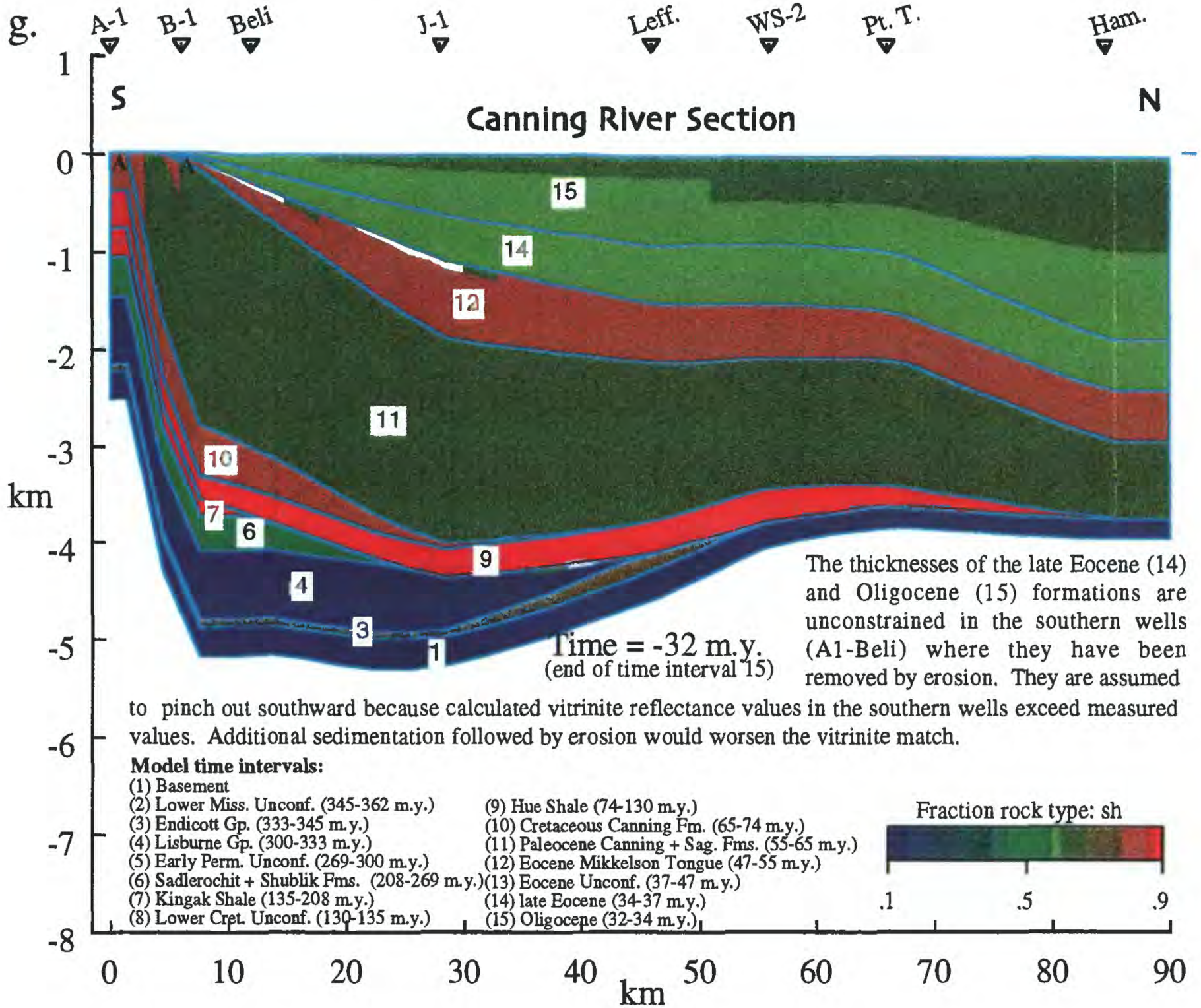

Figure 2. Canning River cross-section; a-i show key 'time slices' in the burial and uplift history of the region.

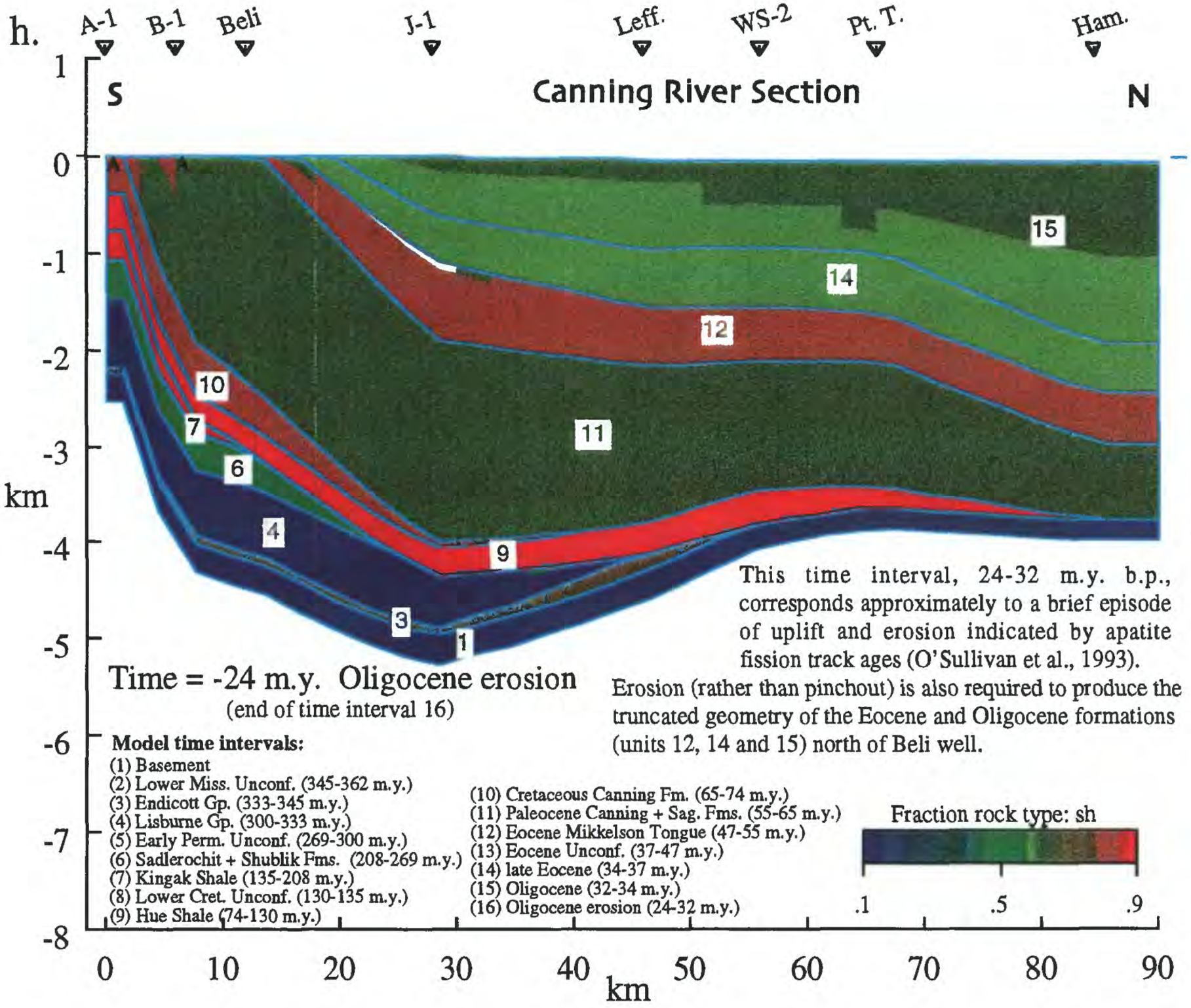

Figure 2. Canning River cross-section; a-i show key 'time slices' in the burial and uplift history of the region.

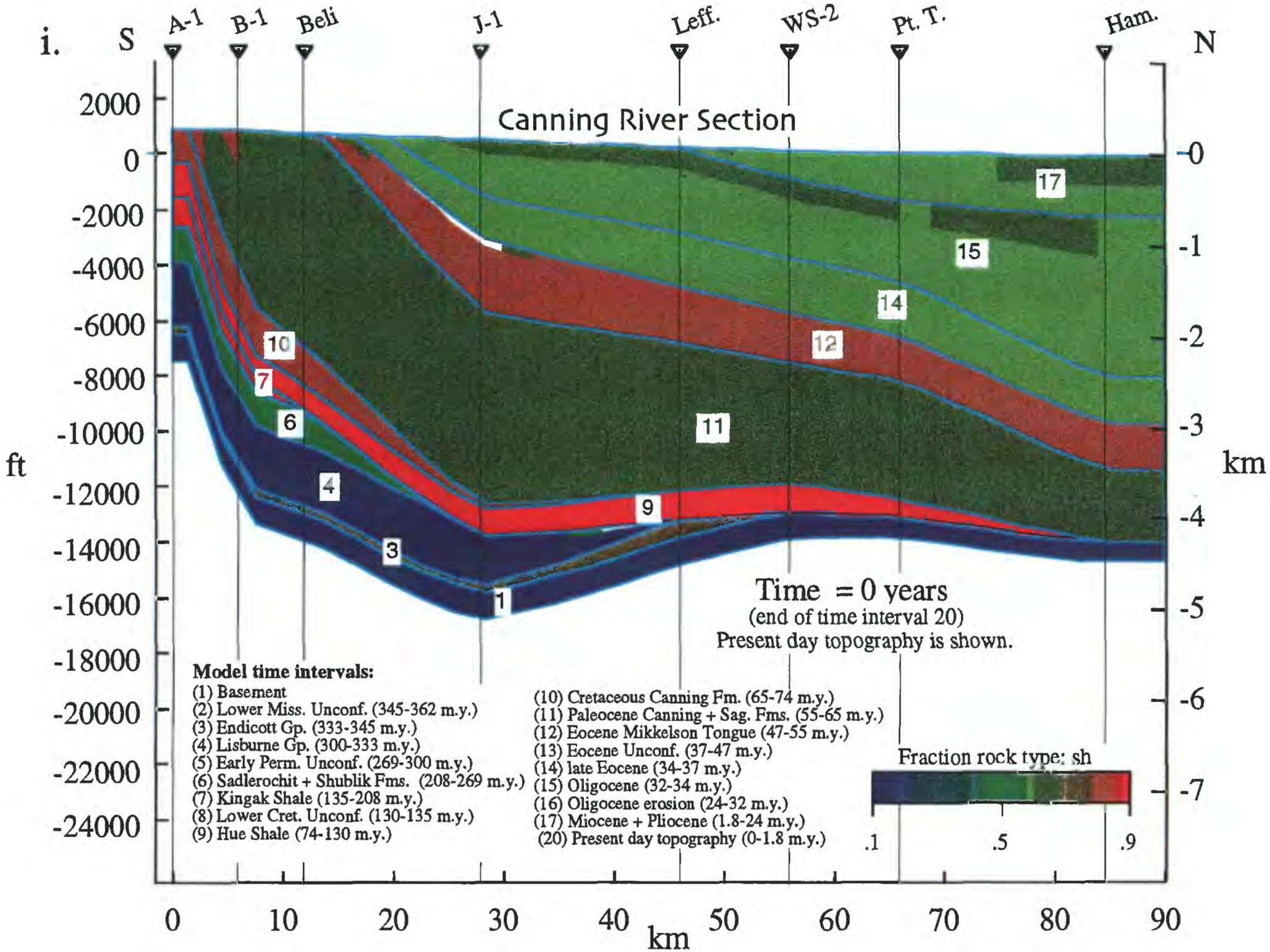

Figure 2. Canning River cross-section; a-i show key 'time slices' in the burial and uplift history of the region.

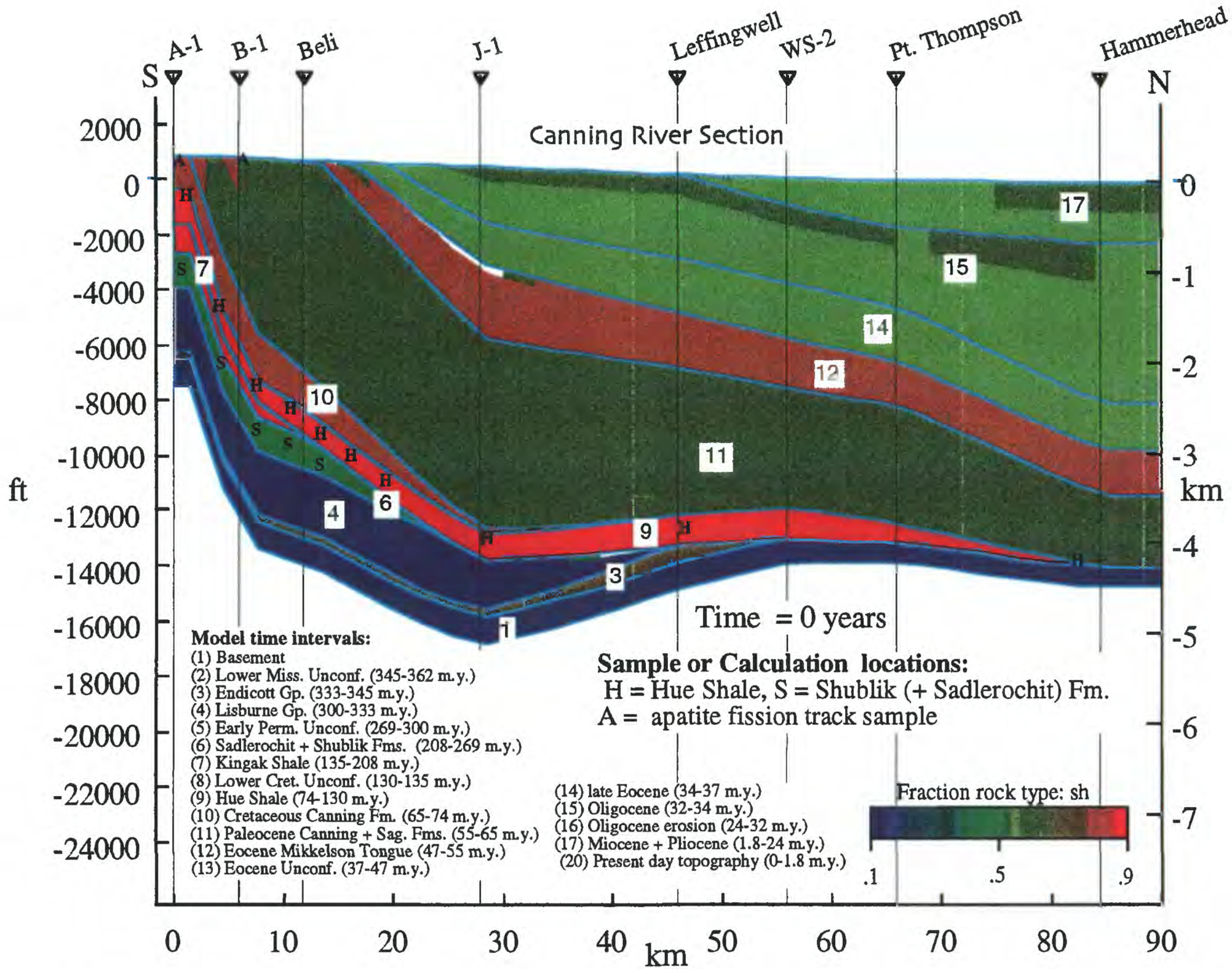

Figure 3. Cross-section showing approximate locations of AFT sample sites (A), and locations of nodes where calculations are reported in the Hue Shale (H), and in the Shublik Fm. (S).

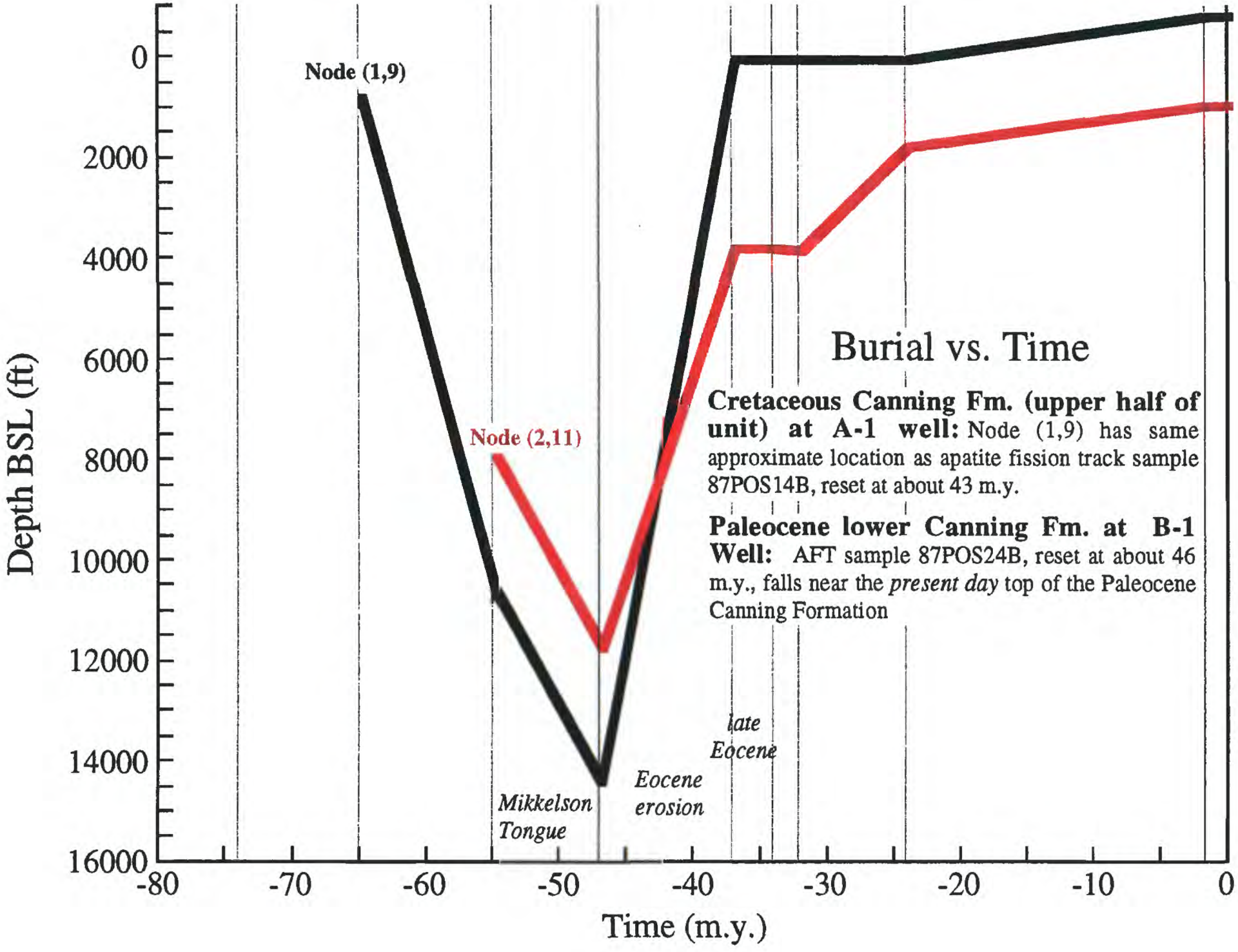

Figure 4. Burial history calculated for two nodes whose positions approximate the locations of AFT samples (see O'Sullivan et al., 1993, Fig. 4).

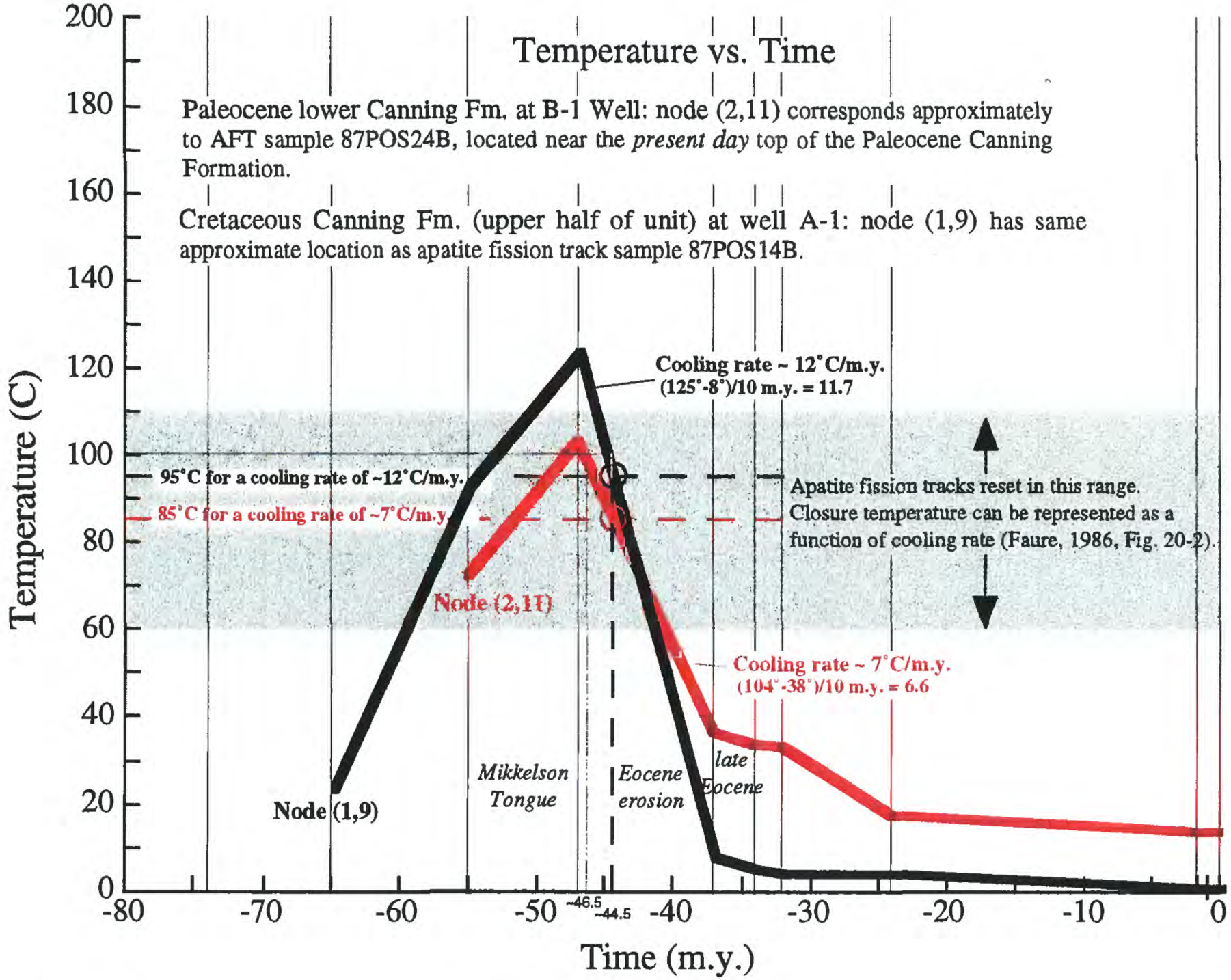

Figure 5. Temperature vs. time calculated for two nodes whose positions approximate the locations of AFT samples (see O'Sullivan et al., 1993, Fig. 4). Closure temperatures determined from cooling rates are based on Faure (1986, Fig. 20-2). See text for discussion.

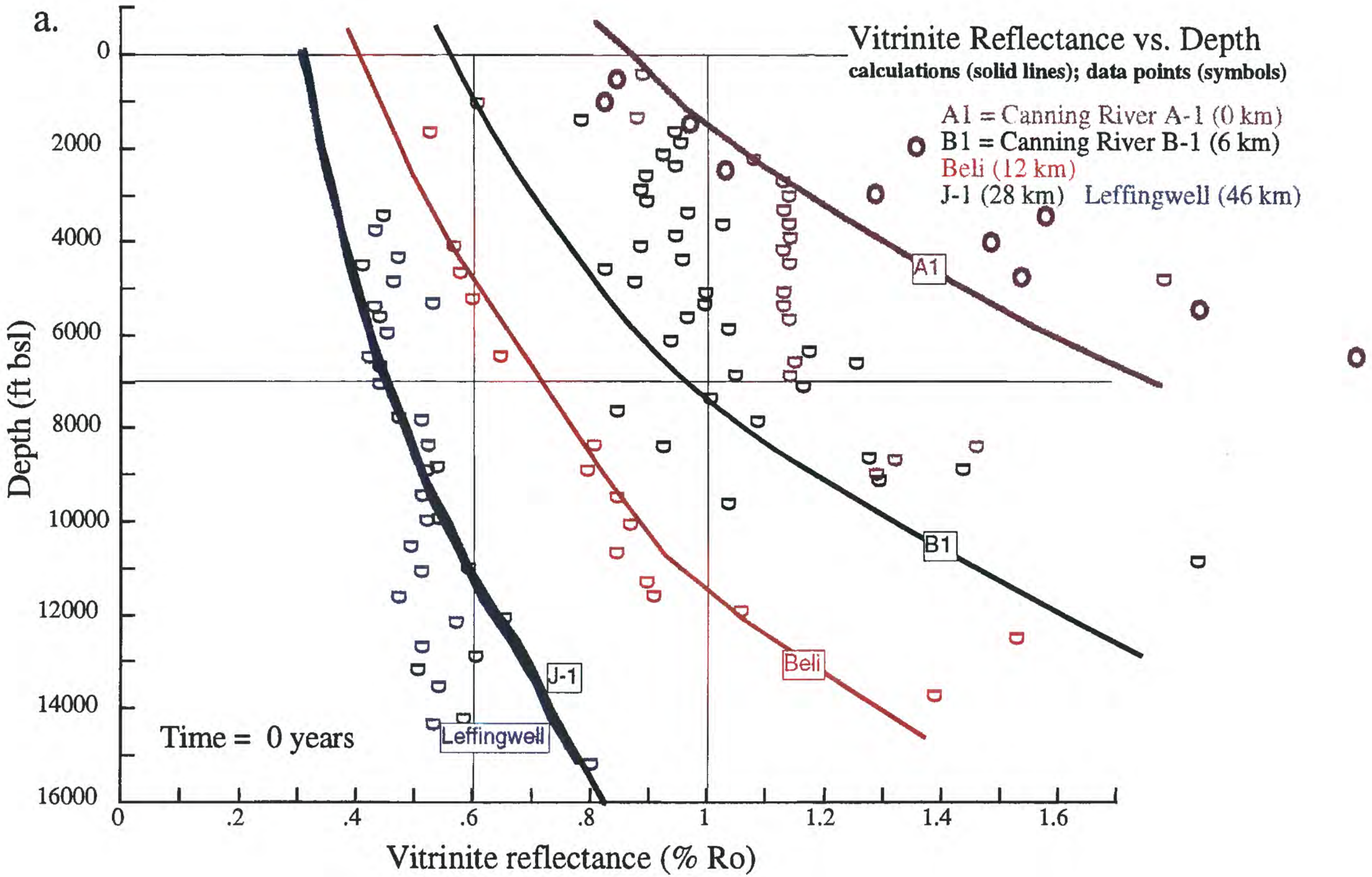

Figure 6. Calculated vitrinite reflectance values a) plotted vs. depth and superimposed on measured values for the four southern wells in the Canning River section, b) for the three northern wells in the section, and c) plotted as contours on the cross section. Vitrinite reflectance data are from Johnsson et al. (1992) and Bird et al. (in prep.). For the Canning River A-1 well circles are a single data set provided by Unocal.

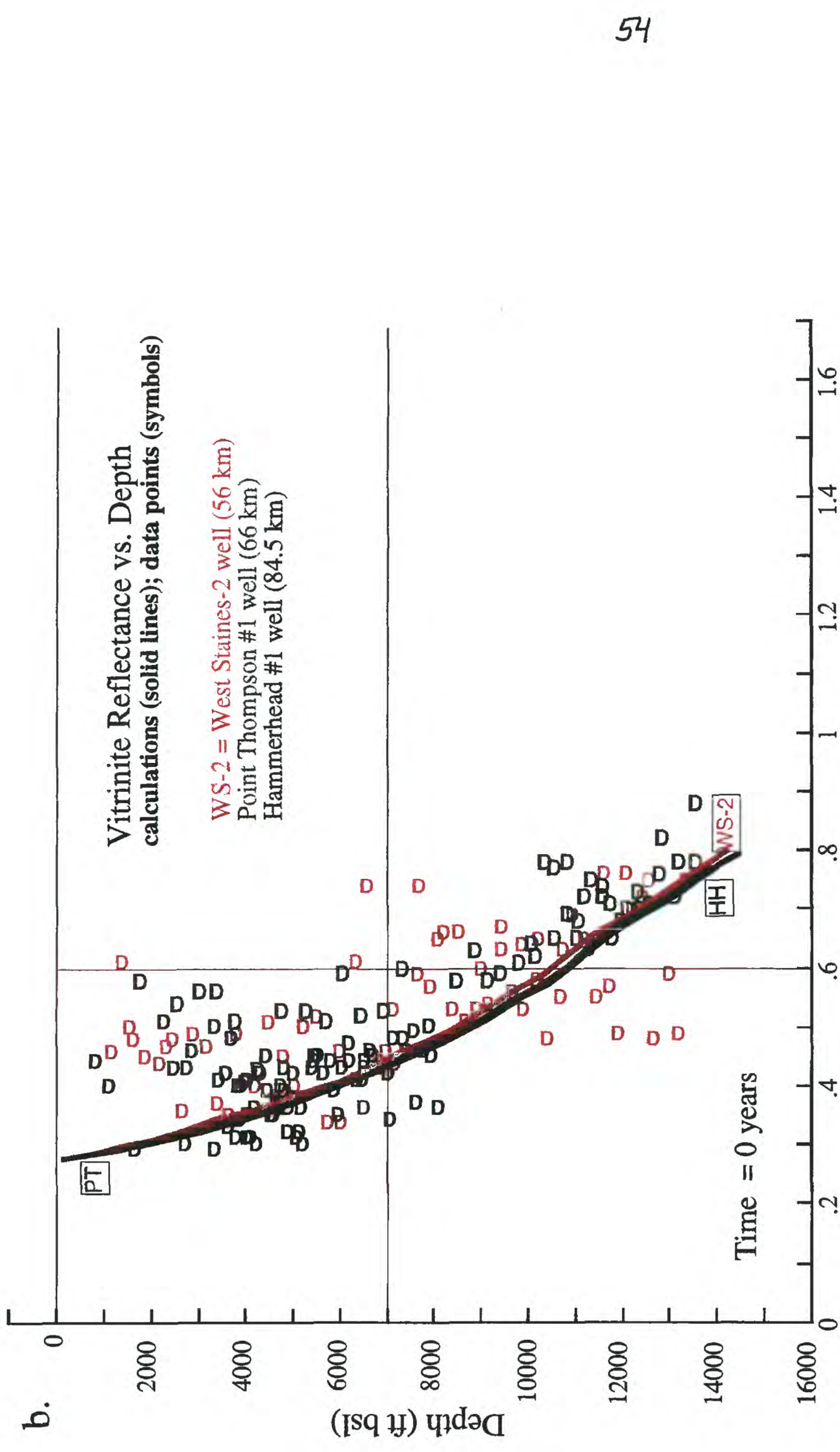

Figure 6. Calculated vitrinite reflectance values a) plotted vs. depth and superimposed on measured values for the four southern wells in the Canning River section, b) for the three northern wells in the section, and c) plotted as contours on the cross section. Vitrinite reflectance data are from Johnsson et al. (1992) and Bird et al. (in prep.).

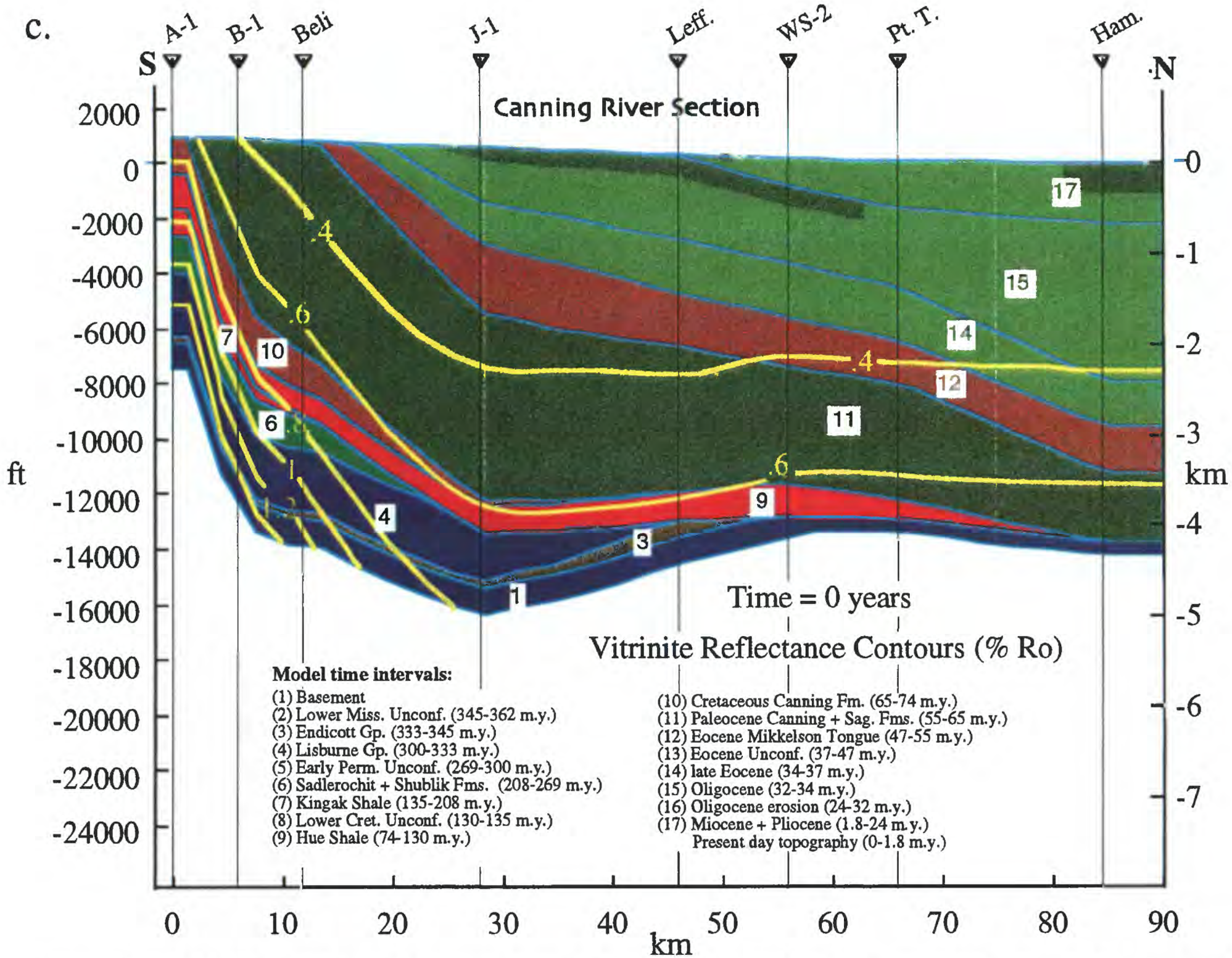

Figure 6. Calculated vitrinite reflectance values a) plotted vs. depth and superimposed on measured values for the four southern wells in the Canning River section, b) for the three northern wells in the section, and c) plotted as contours on the cross section. Vitrinite reflectance data are from Johnsson et al. (1992) and Bird et al. (in prep.).

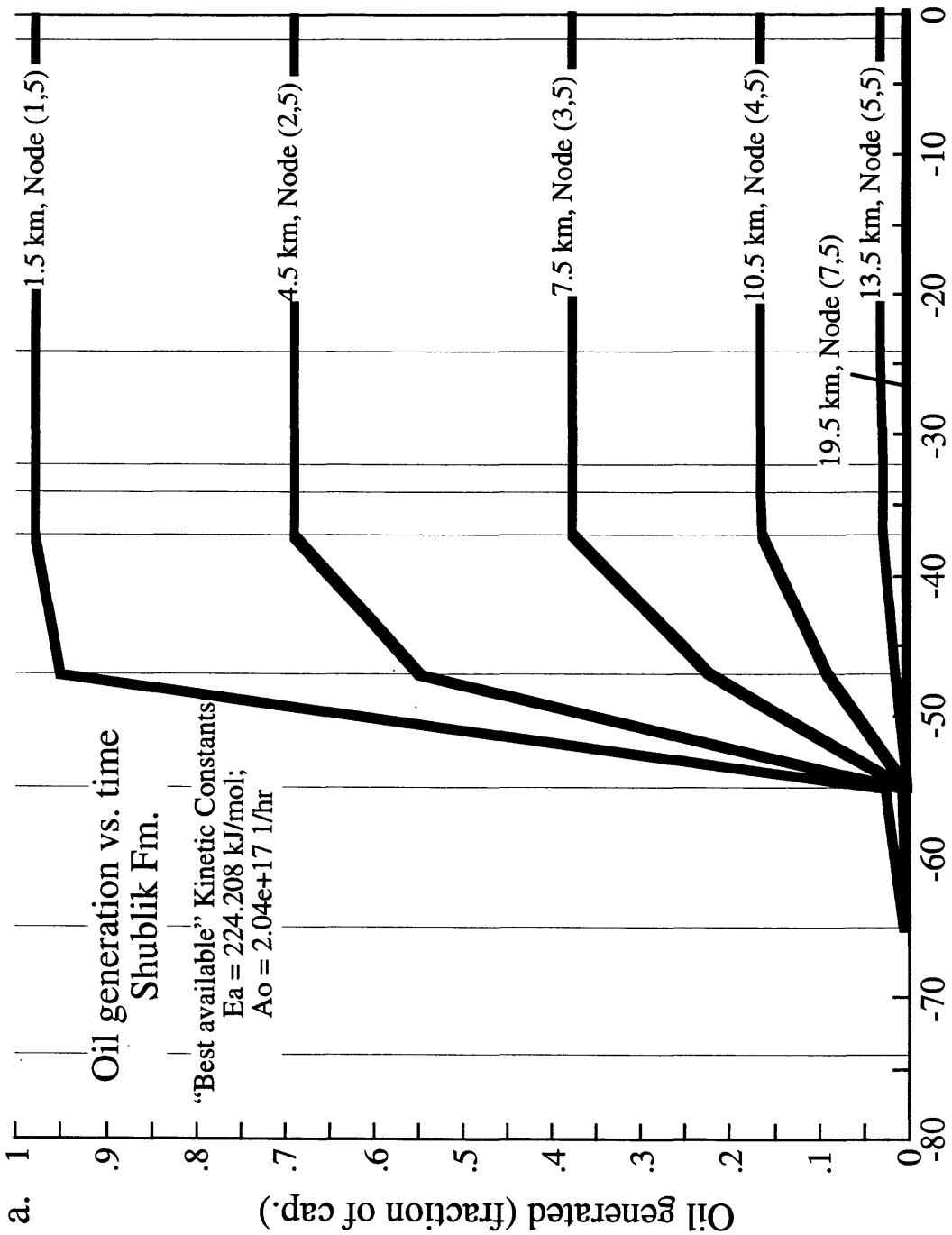

Figure 7. Oil generation vs. time in the Shublik Formation a) using the best available kinetic constants and b) using Phosphoria Shale constants (Table 4).

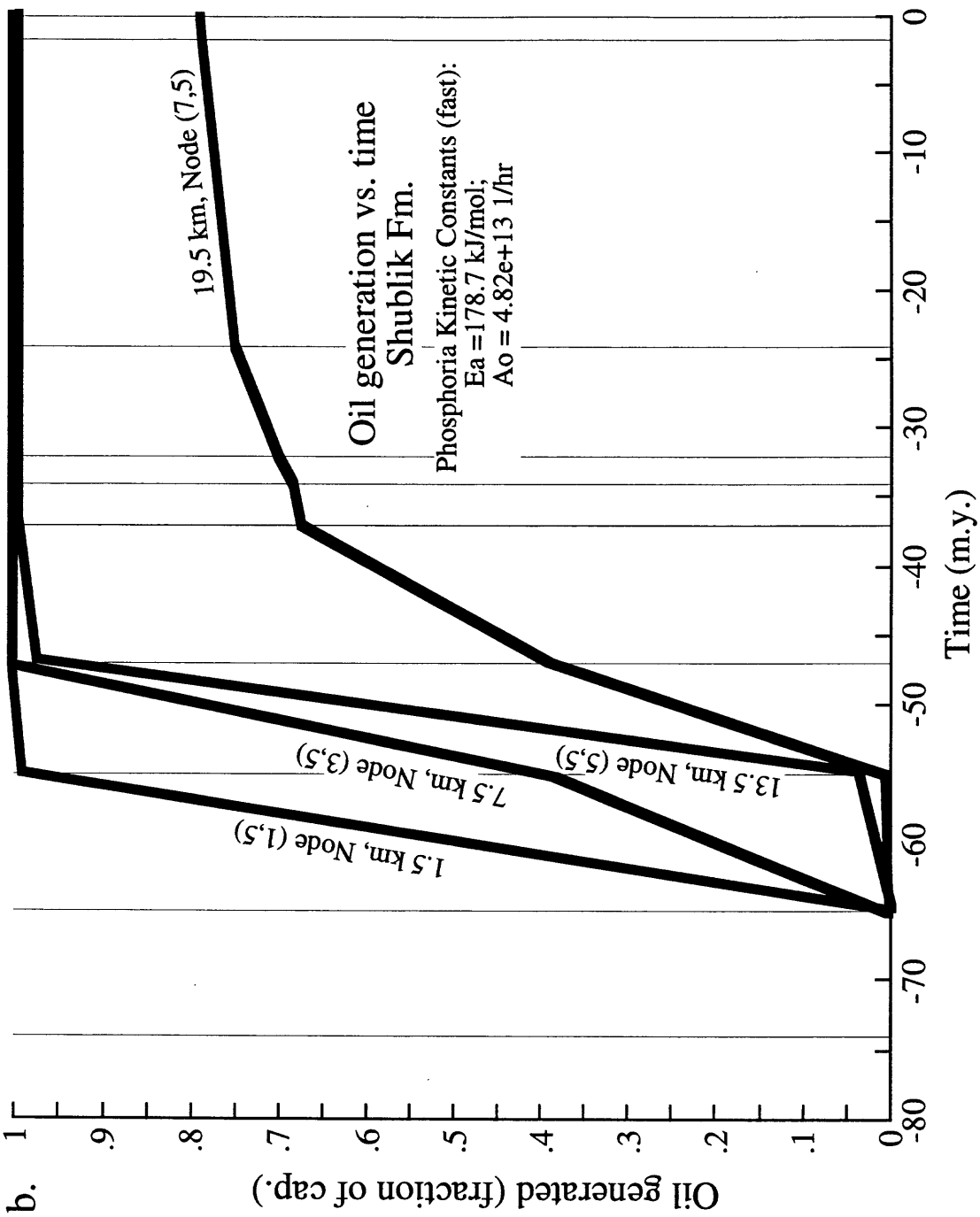

Figure 7. Oil generation vs. time in the Shublik Formation a) using the best available kinetic constants and b) using Phosphoria Shale constants (Table 4).

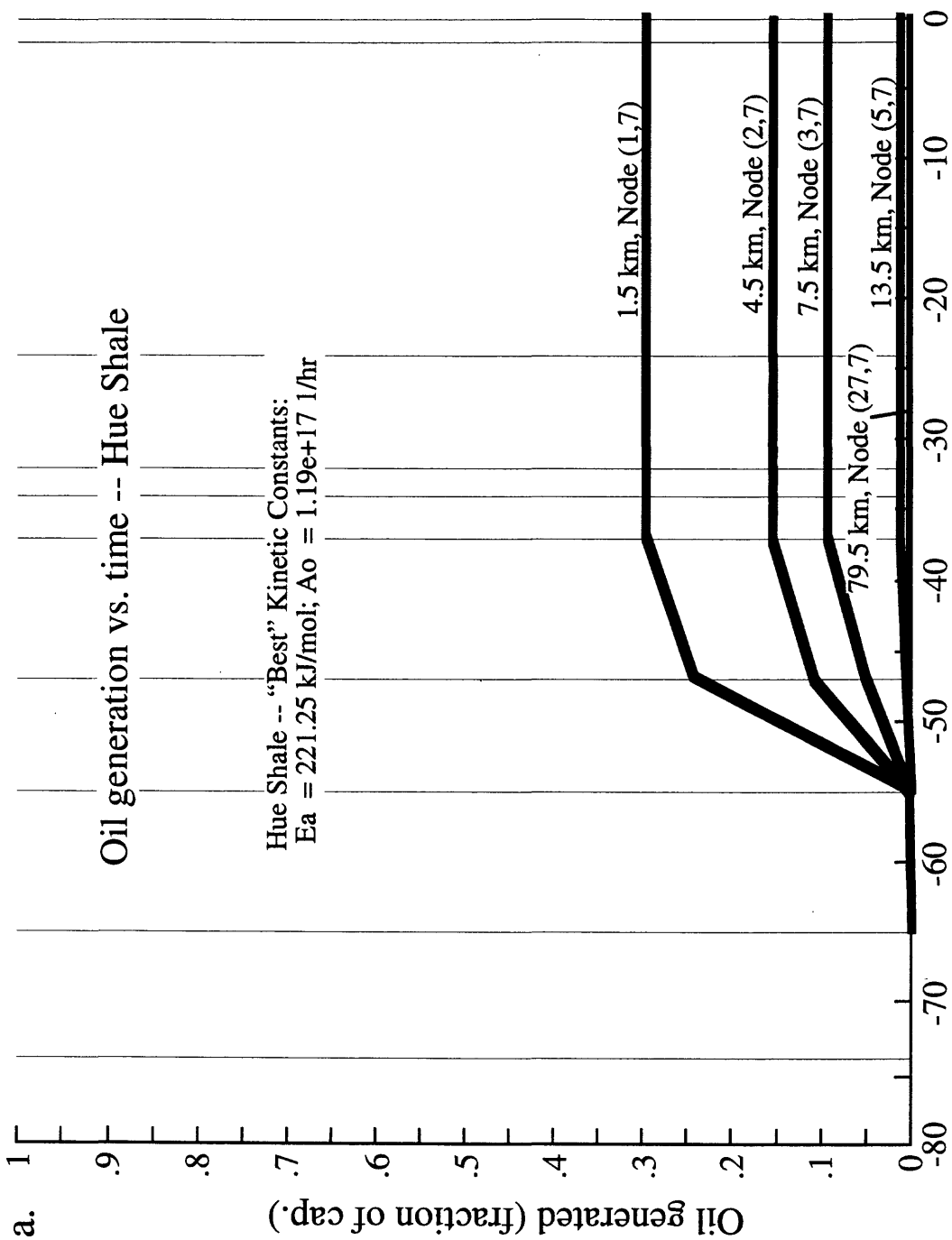

Figure 8. Oil generation vs. time in the Hue Shale a) using the best available kinetic constants and b) using Phosphoria Shale constants (Table 4).

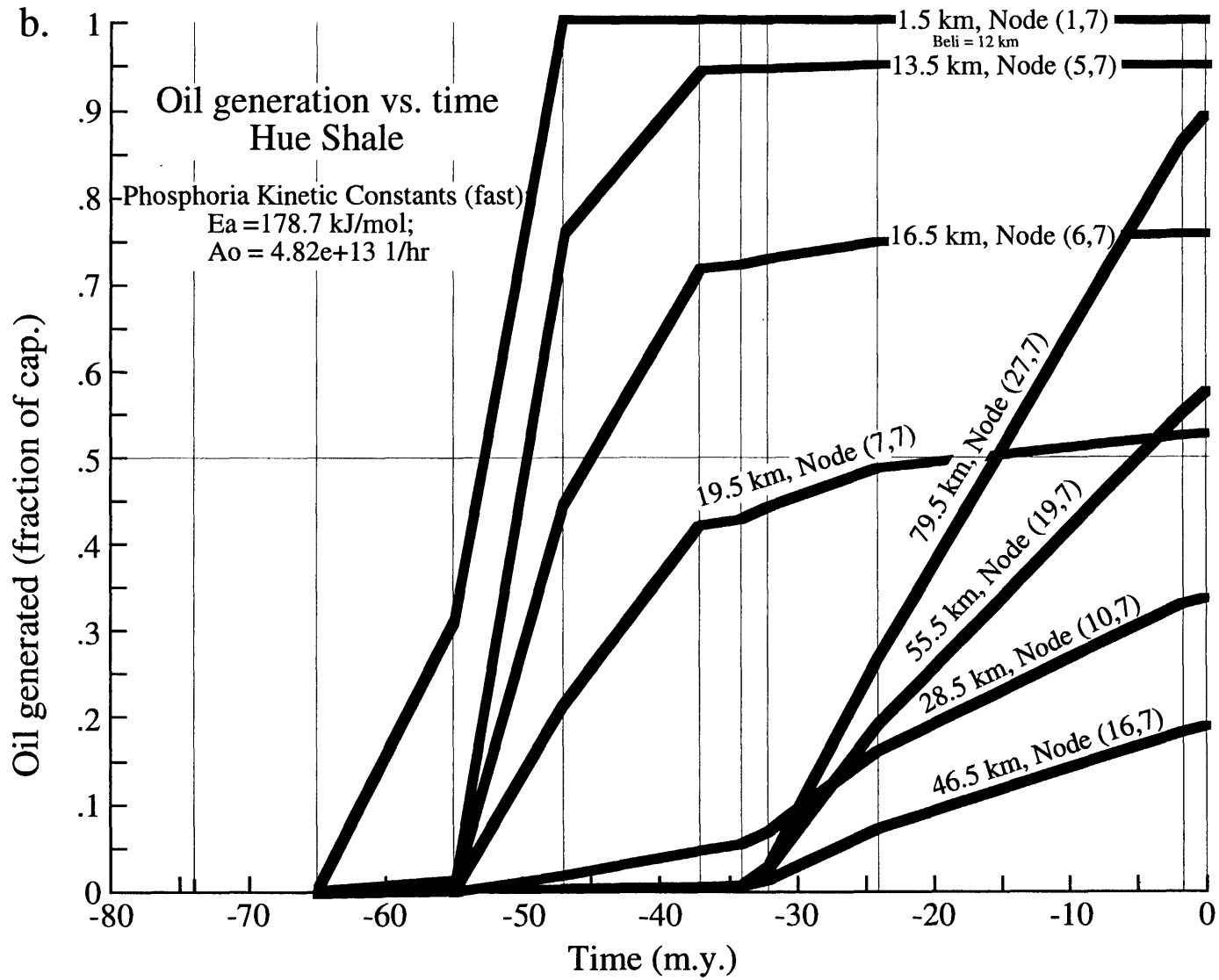

Figure 8. Oil generation vs. time in the Hue Shale a) using the best available kinetic constants and b) using Phosphoria Shale constants (Table 4).

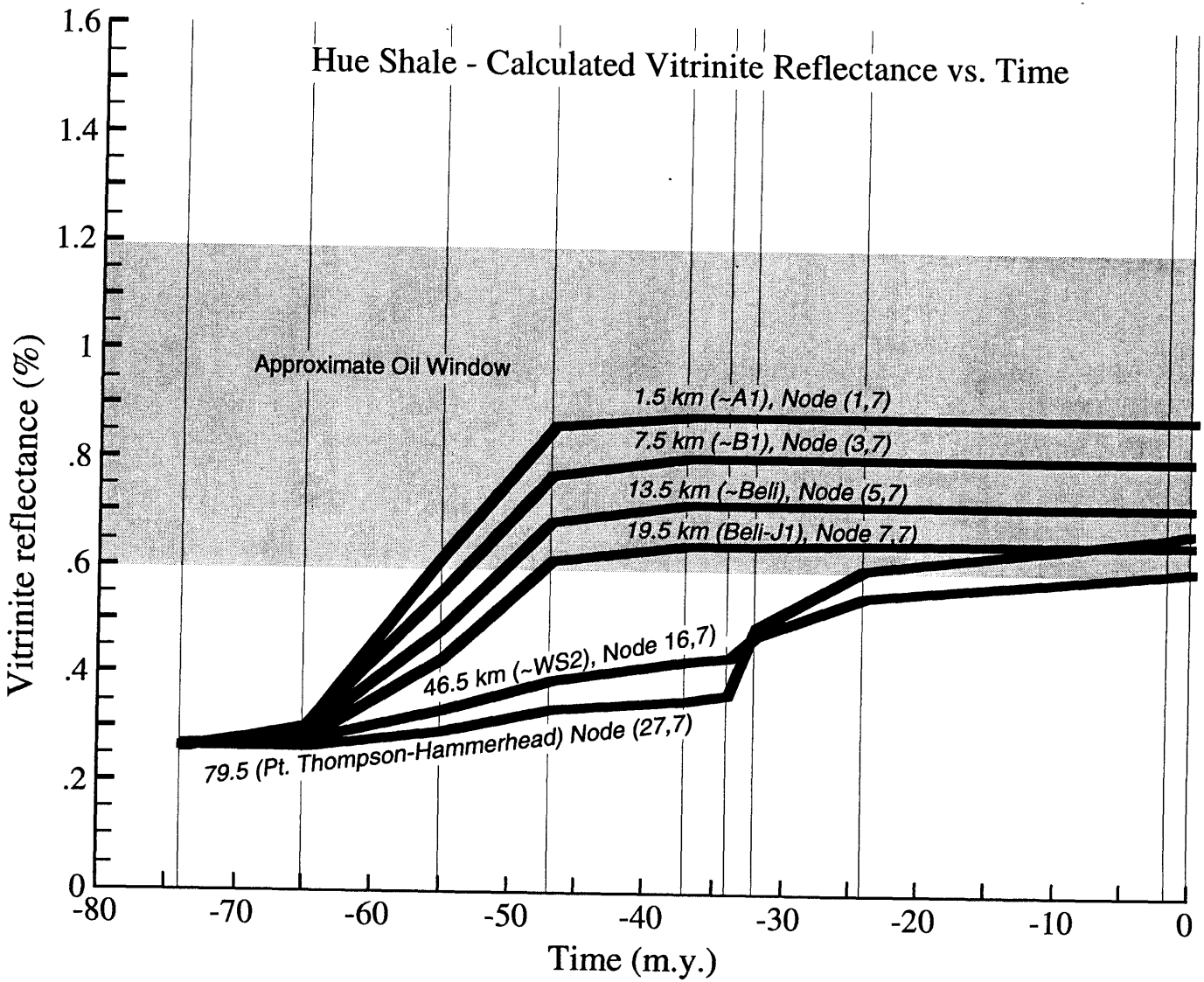

Figure 9. Vitrinite reflectance values vs. time calculated for several locations in the Hue Shale.

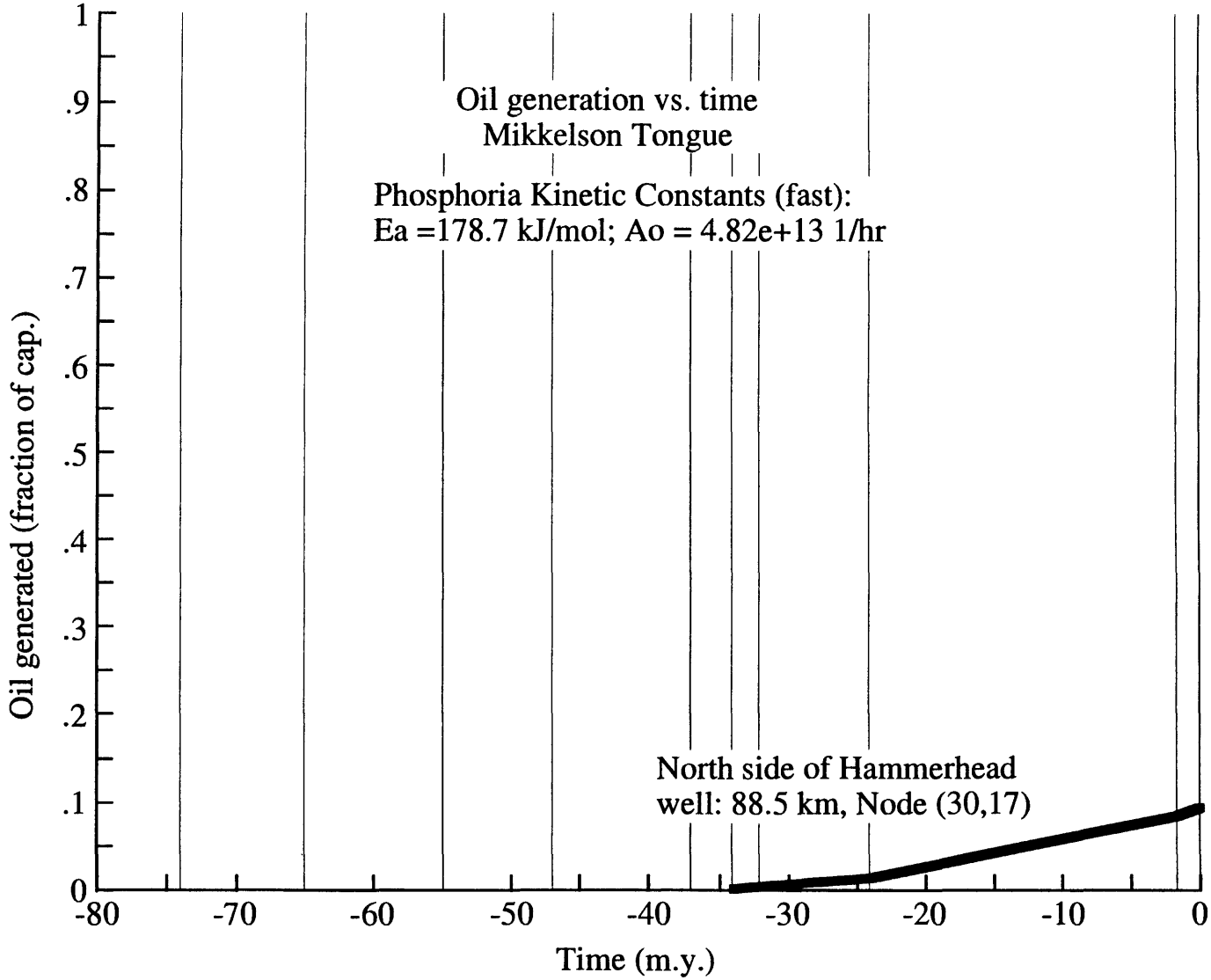

Figure 10. Oil generation vs. time for the Mikkelson Tongue of the Canning Formation using Phosphoria Shale constants. The Mikkelson Tongue has the deepest burial history at node (30, 17) at the north end of the section.